AD-A037 819 VIRGINIA POLYTECHNIC INST AND STATE UNIV BLACKSBURG --ETC F/G 13/13
RELIABILITY STUDY OF SINGER. VOLUME I. VALIDATION OF MODEL.(U)
JAN 77 S M HOLZER, A E SOMERS, J C BRADSHAW F29601-75-C-0050
UNCLASSIFIED AFWL-TR-76-192-VOL-1 NL

1 OF 1
ADA037819

END
DATE FILMED
4-77

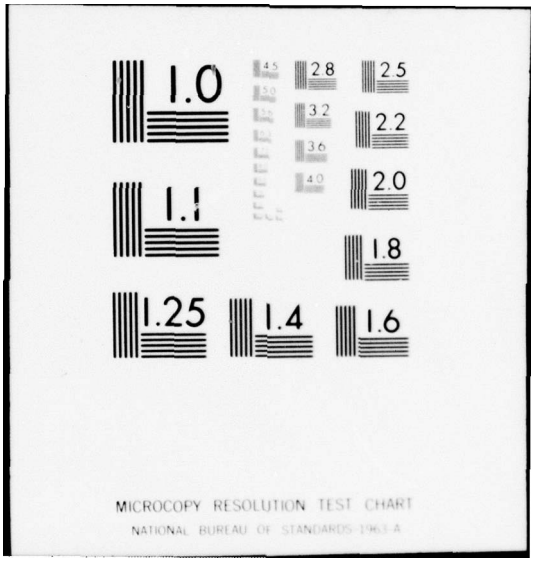
1.0
1.1
1.25
1.4
1.6
1.8
2.0
2.2
2.5
2.8
3.2
3.6
4.0
4.5
5.0
MICROCOPY RESOLUTION TEST CHART
NATIONAL BUREAU OF STANDARDS-1963-A

AFWL-TR-76-192, Vol. I

AFWL-TR-
76-192
Vol. I

RELIABILITY STUDY OF SINGER

Volume I
Validation of Model

DEPARTMENT OF CIVIL ENGINEERING
Virginia Polytechnic Institute and State University
Blacksburg, Virginia 24061

January 1977

Final Report

This research was sponsored by the Defense Nuclear Agency under Subtask Y99QAXSC157, Work Unit 04, Work Unit Title, Strategic Structures Vulnerability/Hardening.

Prepared for
Director
DEFENSE NUCLEAR AGENCY
Washington, DC 20305

AIR FORCE WEAPONS LABORATORY
Air Force Systems Command
Kirtland Air Force Base, NM 87117

This final report was prepared by the Department of Civil Engineering, Virginia Polytechnic Institute, Blacksburg, Virginia, under Contract F29601-75-C-0050, Job Order 5710WDNS, with the Air Force Weapons Laboratory, Kirtland Air Force Base, New Mexico. The former Project Officer was Lt Rodney Galloway. Lt Bradshaw (DES) was the Laboratory Project Officer-in-Charge.

When US Government drawings, specifications, or other data are used for any purpose other than a definitely related Government procurement operation, the Government thereby incurs no responsibility nor any obligation whatsoever, and the fact that the Government may have formulated, furnished, or in any way supplied the said drawings, specifications, or other data is not to be regarded by implication or otherwise as in any manner licensing the holder or any other person or corporation or conveying any rights or permission to manufacture, use, or sell any patented invention that may in any way be related thereto.

This report has been reviewed by the Information Office (OI) and is releasable to the National Technical Information Service (NTIS). At NTIS, it will be available to the general public, including foreign nations.

This technical report has been reviewed and is approved for publication.

Joel C. Bradshaw, III

JOEL C. BRADSHAW III
Lieutenant, USAF
Project Officer

FOR THE COMMANDER

James M Warren

JAMES M. WARREN
Lt Colonel, USAF
Chief, Survivability Branch

Frank J. Leech

FRANK J. LEECH
Lt Colonel, USAF
Chief, Civil Engineering Research Division

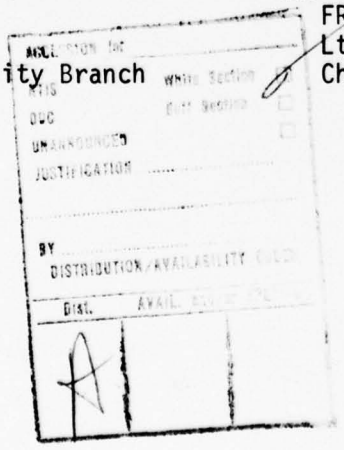

DO NOT RETURN THIS COPY. RETAIN OR DESTROY.

UNCLASSIFIED

SECURITY CLASSIFICATION OF THIS PAGE *(When Data Entered)*

REPORT DOCUMENTATION PAGE		READ INSTRUCTIONS BEFORE COMPLETING FORM
1. REPORT NUMBER AFWL-TR-76-192, Vol I	2. GOVT ACCESSION NO.	3. RECIPIENT'S CATALOG NUMBER
4. TITLE *(and Subtitle)* RELIABILITY STUDY OF SINGER Volume I Validation of Model		5. TYPE OF REPORT & PERIOD COVERED Final Report 6. PERFORMING ORG. REPORT NUMBER
7. AUTHOR(s) S. M. Holzer, A. E. Somers & J. C. Bradshaw, III		8. CONTRACT OR GRANT NUMBER(s) F29601-75-C-0050
9. PERFORMING ORGANIZATION NAME AND ADDRESS Department of Civil Engineering Virginia Polytechnic Institute & State Univ. Blacksburg, Virginia 24061		10. PROGRAM ELEMENT, PROJECT, TASK AREA & WORK UNIT NUMBERS 62704H 5710WDNS
11. CONTROLLING OFFICE NAME AND ADDRESS Director Defense Nuclear Agency Washington, D.C. 20305		12. REPORT DATE January 1977 13. NUMBER OF PAGES 94
14. MONITORING AGENCY NAME & ADDRESS *(if different from Controlling Office)* Air Force Weapons Laboratory (DES) Kirtland Air Force Base, New Mexico 87117		15. SECURITY CLASS. *(of this report)* UNCLASSIFIED 15a. DECLASSIFICATION/DOWNGRADING SCHEDULE

16. DISTRIBUTION STATEMENT *(of this Report)*

Approved for public release; distribution unlimited.

17. DISTRIBUTION STATEMENT *(of the abstract entered in Block 20, if different from Report)*

406 196

18. SUPPLEMENTARY NOTES

This research was sponsored by the Defense Nuclear Agency under Subtask Y99QAXSC157, Work Unit 04, Work Unit Title; Strategic Structures Vulnerability/Hardening.

19. KEY WORDS *(Continue on reverse side if necessary and identify by block number)*

Reinforced Concrete Analysis
Dynamic Analysis
Nonlinear Structural Response
Airblast Effects
Finite Element Method
Energy Minimization
Structural Failure & Collapse

20. ABSTRACT *(Continue on reverse side if necessary and identify by block number)*

The first volume of the report is connected with the refinement and the demonstration of the current capability of the computer code SINGER. The function of SINGER is to predict the complete response (including element failures and strucutral collapse) of skeletal reinforced concrete structures to static and dynamic loads. The refinement of SINGER comprises the following principal tasks: The validation of the finite element, the selection of an appropriate quadrature method, and the formulation of error controls.

OVER

DD FORM 1 JAN 73 1473 EDITION OF 1 NOV 65 IS OBSOLETE

UNCLASSIFIED

SECURITY CLASSIFICATION OF THIS PAGE *(When Data Entered)*

(Blk 20)

in energy evaluations. In the validation effort, the performance of the finite element (and assemblages of the element) is tested over the entire range of response, from the elastic geometrically linear range to the inelastic geometrically nonlinear range. The validation is based on two continuum models of elastic and inelastic beam-columns, which admit closed-form solutions. A literature survey indicated that the Gaussian quadrature is the most appropriate quadrature errors. The selection is based on convergence characteristics and error estimates. Energy computations involve discretization and quadrature errors. Accordingly, error measures are proposed to control the accuracy of the response predictions. A variety of problems is solved and compared to independent numerical and experimental solutions to illustrate the current capability of SINGER.

PREFACE

This is the first volume of a two volume report on the work performed under contract F29601-75-C-0050.

We wish to express our gratitude to the graduate students Dave Stinnett, Ayo Abatan, and Ron Shiflett for their contributions to the project. Our special thanks go to Dr. Richard D. Walker for his counsel and generous support.

CONTENTS

SECTION I

INTRODUCTION

This report is concerned with the refinement of the computer code SINGER, which was developed under contract F29601-73-C-0022. The function of SINGER is to predict the nonlinear response, including member failures and structural collapse, of plane skeletal reinforced concrete structures to static and dynamic loads. The nonlinearities may be caused by finite displacements and inelastic constitutive laws [1].

The mathematical model of SINGER represents an assemblage of one-dimensional finite elements, which simulate the behavior of beam-columns. The model is expressed in the form of an energy function which is defined by the generalized coordinates and forces (external and inertia). The origin of the generalized coordinates corresponds to the unstrained state of the system, the initial state.

The motion (equilibrium path) of the system is determined at a discrete number of points in time (load increments). The solution is extended through successive time steps by the repeated application of the solution process, which comprises the following tasks:

1. The state of the system is defined at the beginning of a time step.
2. The motion during the time step is discretized such that the acceleration at the end of the time step is defined in terms of the initial conditions and the unknown generalized coordinates at the end of the time step.
3. The energy funtion is formulated at the end of the time step and minimized to yield the generalized coordinates.

It follows that the solution contains spatial and temporal discretization errors. Temporal error controls are contained in SINGER [1]. Spatial error controls are proposed in this report.

PURPOSE AND SCOPE

The refinement of SINGER is based on the following principal tasks (sections II - IV): The validation of the finite element, the selection of an appropriate quadrature method, and the formulation of error controls in energy evaluations. These studies motivated the development of a new finite element, which is presented in section V. The current capability of SINGER is demonstrated in section VI, and modifications of SINGER (implemented and proposed) are discussed in section VII.

SECTION II

VALIDATION OF THE FINITE ELEMENT MODEL

This section is concerned with the validation of the macro response of the finite element model of a beam-column.

FINITE ELEMENT MODEL

Beam-column models represent slender elements whose axial and flexural deformations are geometrically coupled. The finite element model of a beam-column, the basic component of the discrete model in SINGER, is based on the following assumptions of the classical beam-column [2, 3]:*

1. The plane of bending coincides with the longitudinal plane of symmetry.
2. Plane sections remain plane and normal to the deformed reference axis.
3. Normal strains and rotations are infinitesimally small.
4. The stress-strain law of any longitudinal fiber is defined by the constitutive law of the material.
5. The effect of shear deformations is negligible.

These assumptions have been substantiated for elastic and inelastic reinforced concrete and steel beam-columns, e.g., [2, 4 , 5]. Accordingly, the classical beam-column provides the basis for validating the finite element model.

It should be noted that in spite of the restriction of the finite element model to small deformations, there are no limitations on the displacements of the nodes to which the elements are connected [1].

VALIDATION BASIS

The effectiveness of the finite element model is judged on the basis of its performance relative to classical continuum models of columns and beam-columns. The performance of the model is measured in terms of micro and

---

* Numbers in brackets designate references.

macro parameters. Micro parameters consist of strains, stresses, and internal-energy densities; macro parameters describe loads, displacements and element energies.

This distinction in model parameters is made to reflect the difference between pointwise and average behavior of discrete models. For instance, Oliveira [6] proved that the potential energy of an assembly of complete and conforming finite elements converges in the limit to the potential energy of the corresponding continuum model. However, this does not guarantee uniform (pointwise) convergence of strains and stresses. Similarly, in the Ritz method, the convergence of a sequence of approximating functions to the exact solution can only be guaranteed in a mean-square (average) sense [7].

VALIDATION PROBLEMS

The performance of the finite element model (and assemblages of the model) is tested over the entire range of response, from the elastic geometrically linear range to the inelastic geometrically nonlinear range.

In this section, the macro response predictions of the discrete element (and system) model are compared with those of two continuum models: the Elastica model [8], and the Jezek model [9]. These continuum models have been selected for the validation purpose because they admit closed-form solutions. The evaluation of the micro response is conducted in sections IV and VI.

The Elastica problem was first investigated by Euler. (A historical discussion is presented by Timoshenko [10]). It is concerned with the solution of the 'exact' differential equation of a buckled column for the elastic curve (the deformed reference axis). The term exact refers to the formulation of the curvature of the elastic curve. Accordingly, assumption 3

of the classical beam-column model is relaxed. However, the remaining assumptions are inherent in the Elastica model. The closed-form solution of the Elastica model is obtained in the form of elliptic integrals [8].

The Jezek model [9] was developed to obtain a rigorous analytical solution to the stability problem of inelastic beam-columns. Karman [3] was the first [2] to investigate the buckling of an inelastic eccentrically loaded column as a stability problem. Karman formulated the differential equation governing the equilibrium path of the column consistent with assumptions 1 through 5 of the classical beam-column. In addition, he assumed that no strain reversals occurred during any stage of the loading process, including the attainment of the limit point. The constitutive law was obtained from a unidimensional compression test. (The eccentricities were small enough to preclude the appearence of tensile strains). The solution was obtained with great precision by numerical integration. Karman's theory and his results were validated by Chwalla in a series of theoretical and experimental investigations [5,11]

Jezek [9] simplified the Karman model by introducing an elastic-plastic stress-strain law. This permitted him to divide the beam-column into subregions of at most three distinct stress states; I. elastic, II. inelastic in compression, III. inelastic in compression and tension . He formulated differential equations for the distinct stress states (2nd order differential equations in the transverse deflection, which are nonlinear for states II and III) and obtained closed-form implicit relations between the load parameter and the transverse deflection. The constants of integration were evaluated by imposing boundary conditions and continuity conditions at the interfaces of the subregions. He presented solutions

for a rectangular beam-column with two loading conditions;(1) eccentrically loaded and (2) concentrically loaded with a concentrated transverse load at the midspan.

Recently,closed-form solutions to Jezek's problems were presented again [12,13]. They differ from Jezek's work as follows: The curvature rather than the transverse deflection is selected as the dependent variable, complex as well as rectangular cross sections are considered, and the axial loads of the beam-column with the concentrated load at the midspan can be applied eccentrically. Aside from that, the models and the solution procedures of the two versions are identical. These publications resulted in a computer program [14] which is used in the validation effort of inelastic beam-columns.

ELASTIC RESPONSE

A detailed study of the macro response of the discrete model in the elastic geometrically linear and nonlinear range, with special attention to the performance of the internal node, is presented in reference 15. A summary of the major results of this successfully completed validation phase is presented below.

The function of the internal node is to make the location of the reference axis independent of the strain state [1]. It was decided [1] that this goal can be accomplished if the finite element is capable of representing a linearly varying normal strain along its reference axis. For this purpose the internal node was introduced.

This study indicates that the internal node does successfully perform its function. The response predictions (micro and macro) are independent of the location of the reference axis; i.e., the reference axis may be chosen to coincide with any longitudinal fiber of the beam-column or may

even be placed outside the beam without altering the response predictions.

A postbuckling analysis of a concentrically loaded elastic column is conducted to evaluate the ability of the finite element model to predict large displacements with high precision. The results of the analysis are presented in figures 1 and 2 for assemblages consisting of 4 and 9 elements, respectively. They indicate that a sequence of finite element approximations converges monotonically to the exact solution of the Elastica model and that any desired degree of accuracy can be attained by refining the element mesh.

INELASTIC RESPONSE

The second Jezek problem [9], a concentrically loaded,simply supported beam-column with a concentrated transverse midspan load (figure 3a), forms the basis of the validation effort in the inelastic geometrically nonlinear range. The solution of the continuum model is obtained via the Lehigh program [14] for various load combinations (for each prescribed axial load the transverse load is varied until the limit load is attained) and finite element mesh sizes. The response is represented by the equilibrium path (the midspan load vs. midspan deflection) and compared with that of the discrete model.

The results presented in figure 4 are characteristic of the test problems studied: The finite element solution expressed by the equilibrium path converges to the exact solution, and the accuracy of the macro response can be controlled via the mesh size.

In the course of this study it became apparent that the finite element model has a tendency to develop a directional preference with increasing deformations. For instance, when the 1-axes of all elements point from left to right (figure 3a), a slight discrepancy in the transverse deflections of nodes 2 and 4 appears at small loads and grows with the load level.

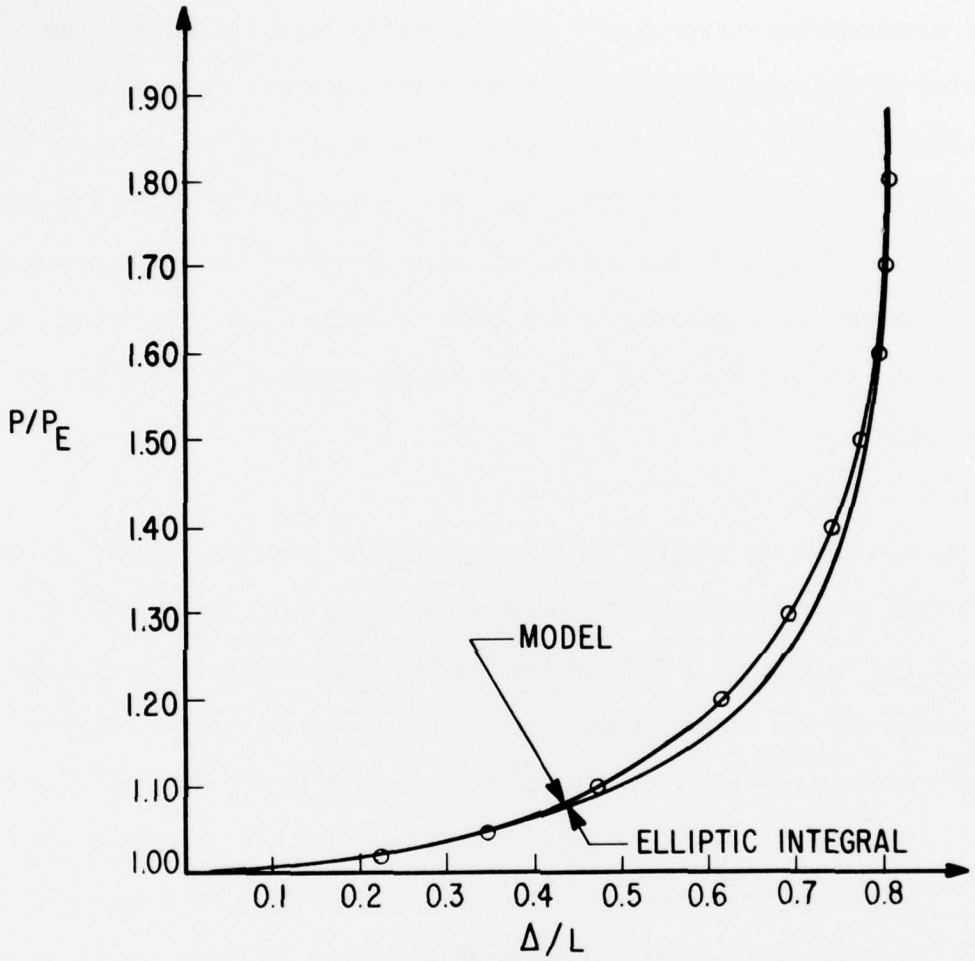

FIG. 1 FOUR-ELEMENT BEAM-COLUMN, CONCENTRICALLY LOADED - TRANSVERSE TIP DISPLACEMENT

3

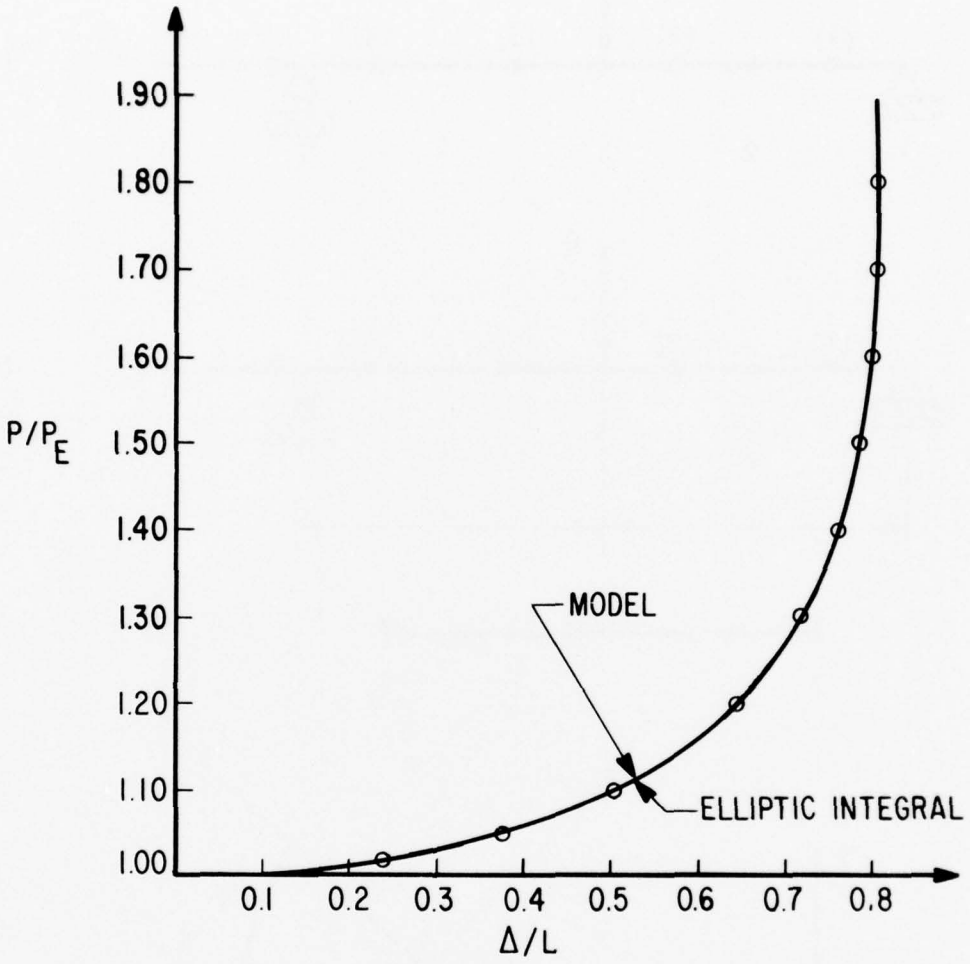

FIG. 2 NINE ELEMENT BEAM-COLUMN, CONCENTRICALLY LOADED - TRANSVERSE TIP DISPLACEMENT

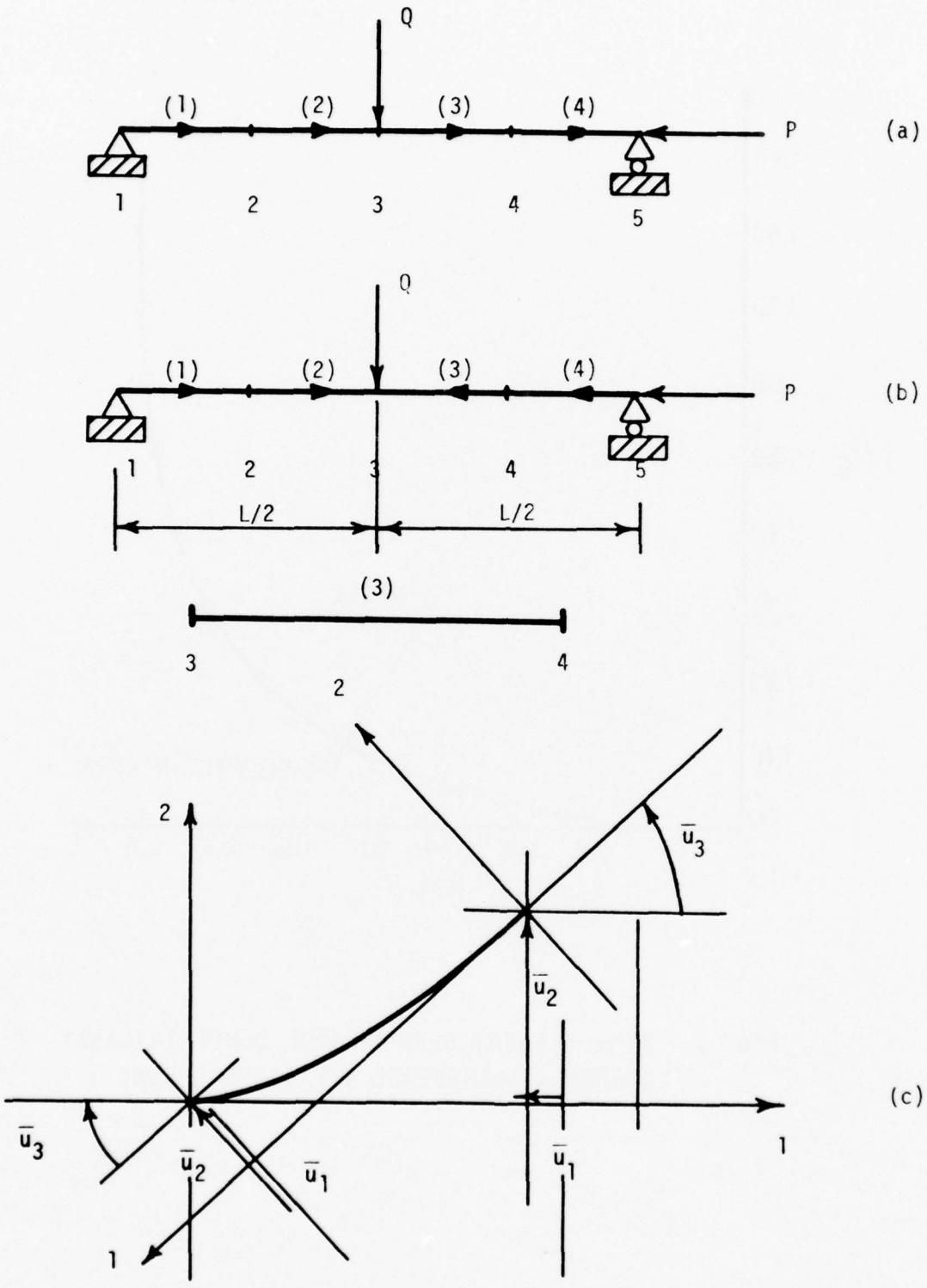

FIG. 3 INELASTIC TEST PROBLEM

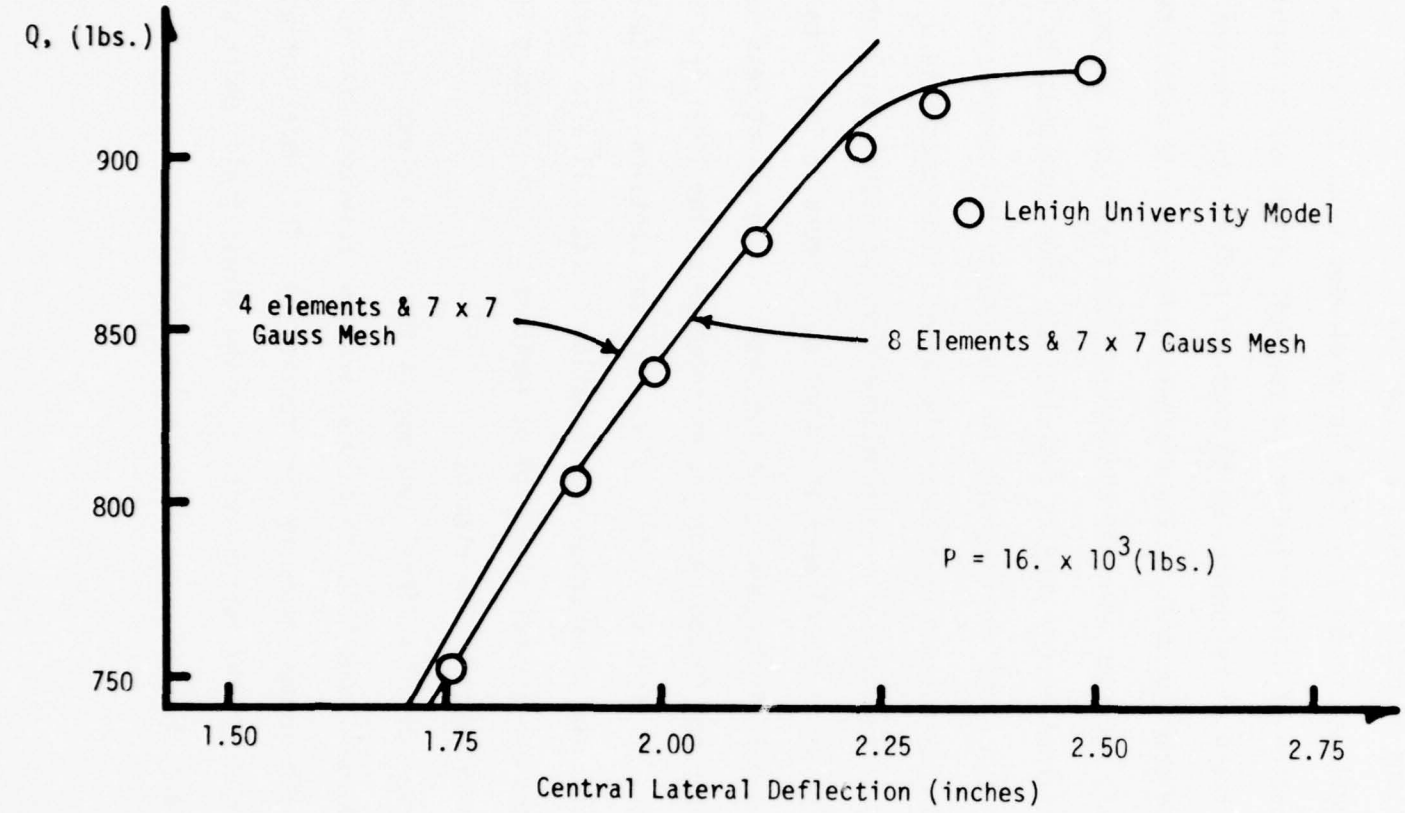

FIG. 4 LEHIGH COMPARISON PROBLEM

On the other hand, when the elements are symmetrically arranged (the 1-axes of all elements point towards the center as in figure 3b), the transverse deflections of nodes 2 and 4 are identical.

The directional tendency of the finite element model appears to result from a combination of discretization and roundoff errors and is magnified by the local frame of reference, which does not reflect the inherent symmetry of the element geometry. The discretization error is associated with the approximate representation of the deformation field (and, hence, the strain and internal-energy density field) of the continuum model by four interpolation functions corresponding to the deformation components $\bar{u}_1, \bar{u}_2, \bar{u}_3, \bar{u}_4$ (rigid-body motions have been eliminated). The components $\bar{u}_1$, $\bar{u}_2$, $\bar{u}_3$ are obtained via coordinate transformations from the global displacements of the nodes to which the element is connected. Figure 3c indicates that for the same nodal displacements, one can obtain two distinct sets of deformation components depending on the orientation of the local 1-axis (left to right, or right to left). Since each set contains inevitable roundoff errors, the corresponding deformation fields will also contain roundoff errors and are not likely to be identical. This accounts for the directional preference of the element.

To minimize the directional tendency of the finite element, a new model has been developed based on a local frame of reference that is intrinsic to the element geometry (see section V). This model contains also a refinement in the representation of the strain field, which was motivated by the study of error controls (section IV).

SECTION III

QUADRATURE METHOD*

This section is concerned with the selection of an integration method to compute the internal energy of the finite element with sufficient accuracy to assure energy convergence. The internal energy of the element is defined by the relation

$$\Pi = \int_V \Pi^* \, dV \tag{1}$$

where the internal-energy density

$$\Pi^* = \int_0^{\varepsilon} \sigma d\varepsilon \tag{2}$$

In Eqs. 1 and 2, V represents the volume of the element, and σ and ε denote the stress and strain at any point in the volume, respectively. Energy evaluations must be performed numerically because of the complex variation of the internal-energy density over the volume of a nonlinear beam-column. A reliable method that requires the least effort to produce a specific degree of accuracy (i.e.,; the "best" quadrature method) is selected to evaluate Eq. 1. A detailed literature search shows that the Gaussian quadrature method is the "best" quadrature method; the selection is based on convergence characteristics and error estimates of several quadrature methods.

There are two basic procedures for evaluating numerically the integral of a function of one variable [16,17]. In the first, points at which the

---

* Prepared by Ayodele Abatan, graduate student, VPI&SU.

function is evaluated are specified a priori at equal intervals, and a polynomial is passed through these function values and integrated exactly. In the second, the sampling points are located so as to achieve maximum accuracy. These two procedures lead to a broad classification of quadrature methods into the following categories:

1 *EQUIDISTANT interpolation-point methods*

2. VARIABLE interpolation-point methods

EQUIDISTANT INTERPOLATION-POINT METHODS

Quadratures possessing equidistant interpolation points are characterized by the Newton-Cotes quadrature. The quadrature formula can be expressed as

$$I = \int_{-1}^{1} f(\xi)\, d\xi = \sum_{i=1}^{n} H_i\, f(\xi_i) + E \qquad (3)$$

where

ξ_i = interpolation points equidistantly spaced over the normalized domain $-1 \leq \xi \leq 1$

H_i = weights

E = error of order $(\Delta)^n$

$\Delta = \frac{2}{n-1}$

n = number of interpolation points

Eq. 3 is obtained by approximating the function $f(\xi)$ with a Lagrange interpolation formula and evaluating the resulting integral exactly. For $n = 3$, Eq. 3 yields

$$I = \frac{1}{3}\,[f(-1) + 4f(0) + f(1)] \qquad (4)$$

which is known as Simpson's rule. Modifications of Simpson's rule and

other rules of equidistant interpolation-point methods are presented in the literature, e.g., [18].

VARIABLE INTERPOLATION-POINT METHODS

The variable interpolation-point methods are known as Gaussian quadratures. Gauss had the ingenious idea [18] to let the interpolation points be variables. Hence for n interpolation points (Gauss points), there are 2n unknowns [ξ_i, $f(\xi_i)$, i = 1, 2, ... n]; which means that an n-point Gaussian quadrature formula is exact for a polynomial of degree 2n-1. Gauss found that by selecting Legendre polynomials as interpolation formulas, he could solve the problem in explicit form. Gaussian quadrature formulas have also been developed for other interpolation formulas [19] such as Hermite, Laguerre, and Jacobi interpolation formulas. The Gaussian-Legendre quadrature formula, a common and highly convergent formula, can be expressed in the form

$$I = \int_{-1}^{1} f(\xi)d\xi = \sum_{i=1}^{n} H_i f(\xi_i) + E \qquad (5)$$

where

ξ_i = Gauss Points

H_i = weights

E = error

The location of Gauss points together with the associated weights are tabulated in the literature, e.g., [19, 20, 21].

The quadratures can also be formulated for multiple integrals:

$$I = \int_{-1}^{1} \int_{-1}^{1} f(\xi,\eta)d\xi d\eta = \sum_{i=1}^{n} \sum_{j=1}^{m} H_i H_j f(\xi_i,\eta_j) + E \qquad (6)$$

where n, m represent the number of Gauss points in the ξ,η direction, respectively.

COMPARISON OF QUADRATURE METHODS

The comparison is based on

a. convergence characteristics

b. error estimates

Equidistant interpolation does not in general lead to a well-convergent process. Convergence is not even guaranteed for functions which have singularities inside the unit circle in a complex plane even though they may be smooth in such a normalized domain. Convergence is more likely for functions which are analytic (i.e., the functions and their derivatives are continuous) within the solution domain [18].

The convergence of the Gaussian quadrature process is guaranteed by the general nature of orthogonal expansions [18]. Many convergence studies and error estimates of the Gaussian quadrature are based on the definite integral

$$\int_a^b w(x)\, f(x)dx \qquad (7)$$

where w(x) is a function for which the moments (or nominal integrals)

$$C_k = \int_a^b w(x)x^k dx, \quad k = 1, 2, \ldots \qquad (8)$$

are defined and $C_o \geq 0$.

4

Gaussian formulas of the form given by Eq. 5 for nonnegative weight functions have several important convergence properties. These properties are the fundamental reasons why Gaussian formulas are so important in applications. These formulas converge to the true value of the integral for almost any conceivable function which one meets in practice. Also the convergence properties for analytic functions show that essentially the only formulas which are interpolatory (i.e. exact for all polynomials of degree $\leq$ n-1 [20])and which converge for all functions analytic in a region of the complex plane containing [a, b] are the Gaussian formulas.

Ivanova [22] presents results concerning the convergence of Gaussian formulas on an infinite segment. Krylov [20] discusses convergence of general quadrature formulas on a finite segment. The following theorem due to Stroud and Secrest [19] is stated here without proof:

> Let w(x) be nonnegative on [a, b] and let f(x) be continuous on this segment. Let $x_i^{(n)}$ and $H_i^{(n)}$, i = 1, 2 .... n, be points and coefficients of the n-point formula of degree 2n-1 for w(x) on [a, b], then

$$\lim_{n \to \infty} \sum_{i=1}^{n} H_i^n \, f(x_i^{(n)}) = \int_a^b w(x)\, dx \qquad (9)$$

Gaussian formulas converge, however, for a wider class of functions than the class of continuous functions. Proofs of this statement are given by Szegö [23]. Several definite statements have been made regarding the usefulness of the Gaussian quadrature method [17,18,21].For example, Lanczos [18] states: "In engineering applications, it happens rather frequently that the average value of a function of unknown structure has to be established on the basis of very few observations. In this case, it is strongly advocated that

the points where the ordinates are measured shall follow the Gaussian pattern. For example, the pressure tubes in an airduct will give much more favorable results if they are not uniformly distributed over the cross-section of the airduct but in conformity with the Gaussian zeros. The same holds for temperature measurements along a wall if the purpose of these measurements is to establish average values."

The error, or remainder, E(f), of the quadrature formula is given by

$$E(f) = \int_a^b w(x)\, f(x)\, dx - \sum_{i=1}^{n} H_i\, f(x_i) \tag{10}$$

Usually error estimates [19] are provided in the form

$$|E(f)| \leq C\, M(f) \tag{11}$$

where C is a constant depending only on the quadrature formula and M(f) is a bound on a quantity related to f(x). For this discussion, M(f) is regarded as a bound on the rth derivative of f(x). Replacing the constant C by e_r, Eq. 11 assumes the form

$$|E(f)| \leq e_r\, M(f) \tag{12}$$

The constants e_r which depend on the quadrature formulas and which must be available to use the estimates are given by Stroud and Secrest [19]. For example, for a Gaussian formula

$$e_r = \frac{1}{r!} \int_a^b w(x)\, [P_n(x)]^2\, dx, \quad 1 \leq r \leq 2n \tag{13}$$

where $P_n(x)$ is a polynomial with the leading coefficient equal to unity, whose zeros are the interpolation points of the quadrature formula.

It has been shown on the basis of Eq. 13 that not only are the Gaussian formulas "best" for integrands of higher order derivatives, but they are also quite accurate for functions having only low order derivatives. Stroud and Secrest [19] showed that for r = 1, 2 the Gaussian formulas are as good as the best formulas which have an equal number of points.

On the basis of the comparison of the Gaussian quadrature method with equidistant methods, it is evident that the Gaussian quadrature method excells not only in regard to its convergence characteristics but also with respect to the associated error estimate for a specified accuracy. Hence,the Gaussian quadrature method is selected as the "best" quadrature method.

SECTION IV

ERROR CONTROLS IN ENERGY EVALUATIONS

The accuracy of the response predictions via SINGER is limited by the accuracy inherent in energy evaluations. The search process for equilibrium states is governed by variations in energy resulting from changes in the generalized coordinates of the finite element model. If these energy variations do not accurately reflect the state of the system, the response predictions are likely to be of poor quality and the solution process may even fail to converge.

There are two types of errors that must be controlled to assure accurate energy evaluations; they are discretization errors and quadrature errors. The discretization error is caused by the representation of the continuum model of a skeletal reinforced concrete structure by an assembly of finite elements. The quadrature error is caused by the numerical integration of the internal-energy density over the volume of the finite element.

In order to control the discretization error, it is necessary to know the convergence characteristics of a sequence of finite element approximations. The finite element model of the beam-column satisfies the conditions of completeness and conformity, which guarantees monotone convergence (in energy) for linear elastic systems [6]. Consequently, in the linear range of response, any refinement of the finite element mesh improves the quality of the energy prediction of the discrete model. However, no general convergence criteria are available for the inelastic range. In this region, convergence characteristics can only be obtained by numerical experimentation.

The quadrature error can be controlled directly by increasing the number of integration points and indirectly by refining the finite element

mesh. If the constitutive law is expressed in polynomial form, the integration points can be selected to achieve exact quadratures. Otherwise, 'exact' integration point distributions can only be obtained by numerical experimentation.

DISCRETIZATION ERROR

A test problem has been selected to study the convergence characteristics of the finite element model over the entire range of response and to establish guidelines for discretization error control. The test problem consists of a single element fixed at one end and subjected to a concentrated moment at the free end. The percent deviation of the extreme fiber strain in compression at the fixed end from the exact value is selected as a measure of the discretization error; i.e.,

$$e_d = \frac{|\varepsilon_c - \bar{\varepsilon}_c|}{|\varepsilon_c|} 100 \tag{14}$$

where e_d is the discretization error measure, ε_c is the exact value, and $\bar{\varepsilon}_c$ is the approximate value of the maximum compressive strain at the fixed end. From Eqs. 2.12 to 2.19 in reference 1, $\bar{\varepsilon}_c$ can be expressed as

$$\bar{\varepsilon}_c = \varepsilon_c^a + \varepsilon_c^b \tag{15}$$

where

$$\varepsilon_c^a = (4\bar{u}_4 - \bar{u}_1)/L \tag{16}$$

and

$$\varepsilon_c^b = -(6\bar{u}_2/L - 2\bar{u}_3)/L \tag{17}$$

The reference axis coincides with the centroidal axis of the cross-section, which is a 2 inch square.

In Eqs. 16 and 17, $\bar{u}_1$, $\bar{u}_4$ represent axial displacements and $\bar{u}_2$, $\bar{u}_3$ represent bending displacements.

This test problem has been selected from a group of problems representing various boundary conditions and end-forces (including axial and shear forces) because it produced the largest discretization error.

ELASTIC RANGE

Figure 5 indicates that the discretization error decreases monotonically with the element length. However, for a given element length, the discretization error increases with ε_c. This is primarily due to the coupling of axial and flexural deformations, which accounts for one source of geometric nonlinearity in the finite element model (the formulation of conditions of equilibrium for the deformed state accounts for the second source).

Further insight into the convergence characteristics of the finite element model can be gained by separating the axial and flexural strain components as indicated by Eq. 15. The results are presented in Table 1 for three slenderness ratios. They indicate that in the limit $\varepsilon_c^b \to \varepsilon_c$ and $\varepsilon_c^a \to 0$, which agrees with the boundary conditions. However, for a given element length, the axial deformation term, ε_c^a, accounts for a major share of the discretization error. For example, if L/r = 208 and M = 6 kip inches, the discretization error without ε_c^a is 2%, but with ε_c^a it is 14.7%. Moreover,the term ε_c^a grows rapidly with the flexural deformations of the finite element, i.e., with the degree of geometric nonlinearity. For example, if L/r = 208 and the moment increases from 6 to 36 kip inches, ε_c^a increases relative to ε_c from 16.7% to 48.9%.

The dominant effect of the term ε_c^a on the strain state can be explained with the aid of Eq. 2.12 in reference 1 . For this particular problem, the

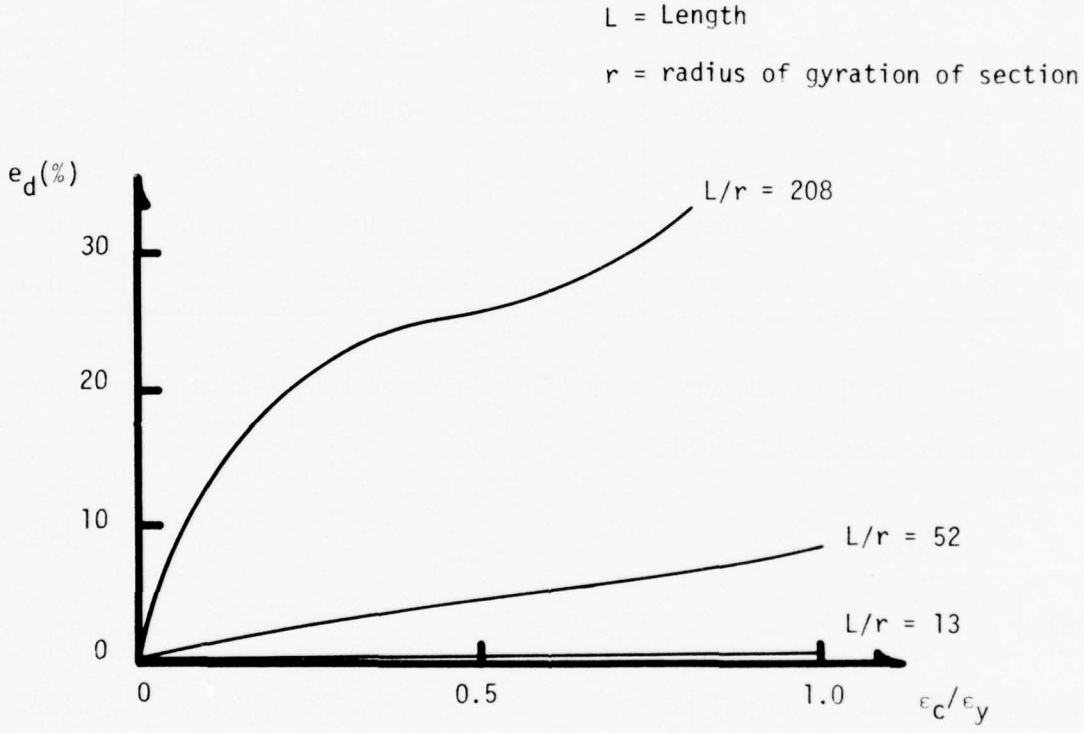

FIG. 5 DISCRETIZATION ERROR
(ELASTIC RANGE)

Table 1. - DISCRETIZATION ERROR

L/r	M kip inches	$\varepsilon_c(10^3)$	$\bar{\varepsilon}_c(10^3)$	$\varepsilon_c^b(10^3)$	$\varepsilon_c^a(10^3)$	e_d (%)
208	6.0	-0.150	-0.128	-0.153	0.025	14.7
52	6.0	-0.150	-0.148	-0.150	0.002	1.3
13	6.0	-0.150	-0.150	-0.150	0.000	0.0
208	36.0	-0.900	-0.620	-1.060	0.440	31.1
52	36.0	-0.900	-0.843	-0.903	0.060	6.3
13	36.0	-0.900	-0.896	-0.900	0.004	0.4

normal strain on the centroidal axis of the element (the ξ-axis) should be zero. However, Eq. 2.12 yields:

$$\varepsilon(\xi,0) = \varepsilon^a + \varepsilon^c \tag{18}$$

where

$$\varepsilon^a = (\Phi_1'\bar{u}_1 + \Phi_4'\bar{u}_4)/L \tag{19}$$

and

$$\varepsilon^c = \frac{1}{2}(\Phi_2'\bar{u}_2/L + \Phi_3'\bar{u}_3/L)^2 \tag{20}$$

It can be seen from Eqs. 2.13 - 2.19(in reference 1) that ε^a and ε^c are polynominals in ξ of order 1 and 4, respectively. Hence, the normal strain cannot vanish identically on the centroidal axis unless the two polynominals are of the same order. For instance, the order of the polynominal of ε^a could be increased from 1 to 4. But this would require 3 additional internal nodes, which would increase the number of degrees of freedom of the finite element

from 7 to 10. The question of the effect of additional internal nodes on the efficiency of the finite element model and the selection of an optimal number of internal nodes is under study. As an alternate solution, the order of the polynomial of ε^c could be reduced from 4 to 1. This approach has been adopted in the new finite element model presented in section V.

INELASTIC RANGE

Figure 6 indicates that in the inelastic range convergence is no longer monotone. Furthermore, the discretization error does not increase monotonically with the value of the extreme fiber strain in compression. Hence, in the inelastic range, refinement of the finite element mesh no longer guarantees uniform improvement in response predictions.

QUADRATURE ERROR

The Gauss-Legendre quadrature is used to evaluate the internal energy of the finite element, which is defined by the relation

$$\pi = \frac{V}{4} \int_{-1}^{1} \int_{-1}^{1} \pi^*(\xi,\eta) d\xi d\eta \tag{21}$$

where

$$\pi^* = \int_0^{\varepsilon} \sigma d\varepsilon \tag{22}$$

In Eqs. 21 and 22, V is the volume of the element; π^* is the internal energy density at any point (ξ,η) of the longitudinal plane of the element; ξ,η are the normalized coordinates in the longitudinal and transverse direction, respectively; and σ,ε denote stress, strain at any point (ξ,η). Eq. 21 may be resolved into two 1-dimensional integrals as follows:

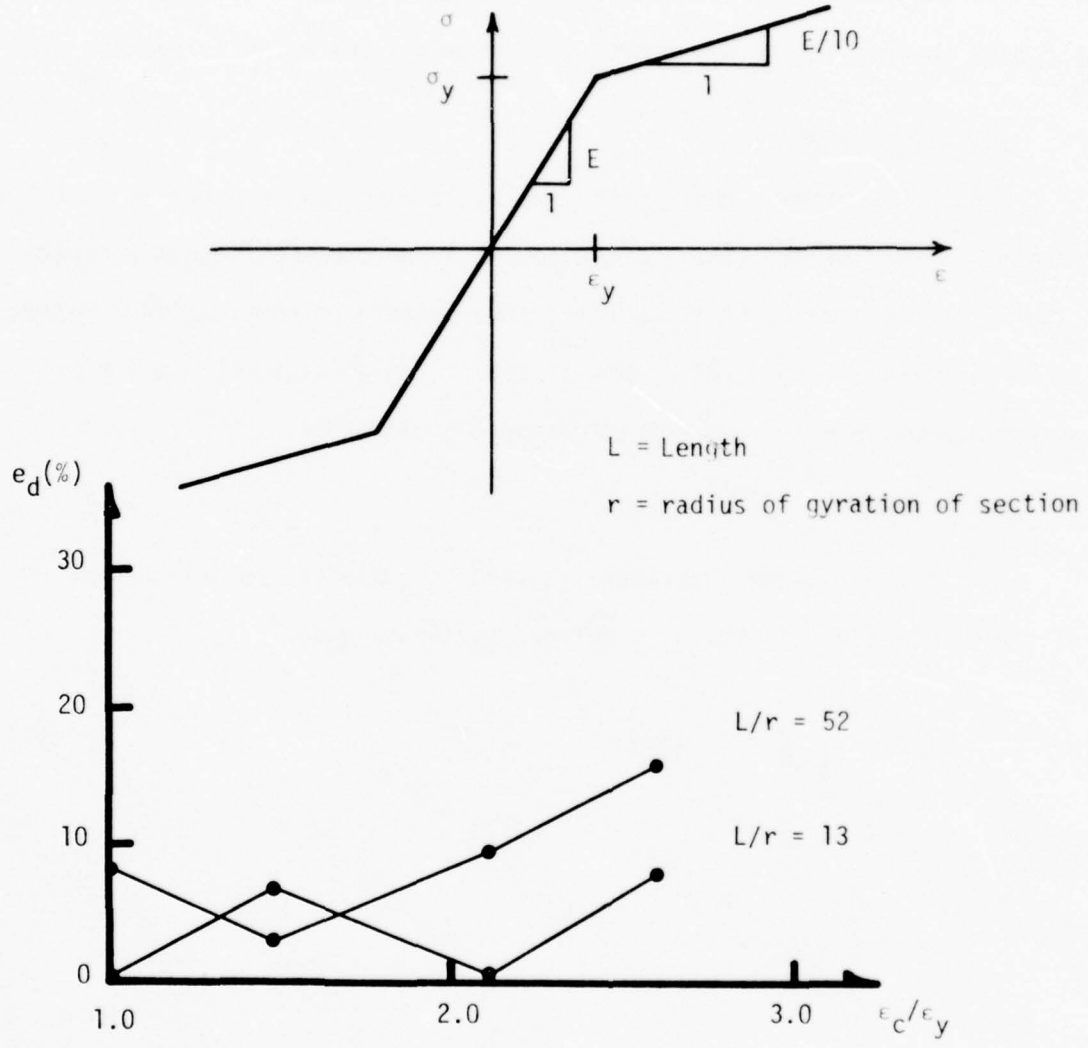

FIG. 6 DISCRETIZATION ERROR
(INELASTIC RANGE)

$$\pi = \frac{L}{2} \int_{-1}^{1} \pi^*(\xi) d\xi \tag{23}$$

and

$$\pi^*(\xi) = \frac{A}{2} \int_{-1}^{1} \pi^*(\xi,\eta) d\eta \tag{24}$$

where $\pi^*(\xi)$ is the internal energy per unit length of the element; A is the cross-sectional area and L is the length of the element. Eqs. 23 and 24 can be expressed via the Gaussian quadrature formula in the form

$$\pi = \frac{L}{2} \sum_{i=1}^{n} H_i \pi^*(\xi_i) \tag{25}$$

and

$$\pi^*(\xi) = \frac{A}{2} \sum_{j=1}^{m} H_j \pi^*(\xi,\eta_j) \tag{26}$$

Substitution of Eq. 26 into Eq. 25 yields the quadrature formula for Eq. 21:

$$\pi = \frac{V}{4} \sum_{i=1}^{n} \sum_{j=1}^{m} H_i H_j \pi^*(\xi_i,\eta_j) \tag{27}$$

where H_i and H_j are the weights, and ξ_i, η_j are the Gauss points (interpolation points) in the longitudinal and transverse direction, respectively.

EXACT QUADRATURE

If the internal energy density is described by a polynomial, one can determine the number of Gauss points required to produce exact quadratures. Suppose the constitutive law is expressed in polynomial form such that the stress, σ, is a polynomial in the strain, ε, of order p. It follows from Eq. 22 that the internal energy density is a polynomial in ε of order p+1. Since the strain is a polynomial in ξ and η of order 4 and 1, respectively (see Eq. 2.12 in reference 1), the strain energy density is a polynomial in ξ and η of order 4(p+1) and (p+1), respectively. Finally, since it takes n Gauss points to integrate a polynomial of order 2n-1 exactly, the number of Gauss points required for an exact energy quadrature is

$$n = (4p+5)/2 \tag{28}$$

in the ξ-direction and

$$m = (p+2)/2 \tag{29}$$

in the η-direction, where p denotes the order of the polynomial representing the stress as a function of strain.

Since the strain field of the new finite element model (section V) is described by a polynomial of order 1 in ξ and η, Eq. 29 is valid for both directions of the new finite element.

ELASTIC RANGE

If Hooke's law is valid (i.e., if p=1), exact energy quadratures can be achieved with the old finite element model (see reference 1) for n=5, m=2 and with the new finite element model (see section V) for n=m=2.

INELASTIC RANGE

Since the constitutive laws in SINGER are not described by polynomials (only by piecewise linear functions), exact Gauss rules (Gauss dis-

tributions) cannot be defined in the inelastic range even for monotonic loading. In any case, the possibility of strain reversals (hysteretic response) makes the polynomial representation of the complete constitutive law unlikely.

Since the internal-energy density function, π^*, cannot be described analytically in the inelastic range, formulas to estimate quadrature errors cannot be applied (they require knowledge of at least the first order derivative of π^*, e.g., [18]). Hence, error estimates can only be obtained by numerical experimentation. For instance, one can establish an 'optimal' Gauss rule, defined as the minimum Gauss rule required to obtain the maximum quadrature accuracy consistent with the computer accuracy, and assess the quadrature accuracy of coarser rules relative to the optimal rule. This approach has been used with the aid of a streamlined computer program that has variable Gauss rules. (Note that presently the Gauss rules in SINGER are fixed).

LONGITUDINAL GAUSS RULE

Quadrature-discretization error studies of the 'test' problem in the elastic and inelastic range indicate that the longitudinal quadrature error corresponding to the 3-point rule of SINGER is always significantly below the discretization error. Consequently, it appears that the longitudinal quadrature error can be controlled indirectly via the discretization error. However, since it may be more efficient to control the two errors independently, and since this observation may not always be true, it is recommended that variable Gauss rules be introduced in SINGER.

TRANSVERSE GAUSS RULE

A quadrature error study of the internal energy per unit length as

defined by Eq. 24 is based on the reinforced concrete section of reference 25 (see figure 8). The purpose is to determine the accuracy of the fixed transverse rule in SINGER relative to the optional rule for a wide range of inelastic deformations (see figures 2 and 6 in Vol. II for a description of the Gauss point locations used in SINGER). The results of this study indicate that the fixed rule in SINGER is quite accurate for predicting the total energy stored in the cross-section. However, it may cause large errors in predicting the energy stored in the confined region of the cross-section. For instance, for a given strain distribution, the quadrature error in the total energy is 2.3%, but the error in the energy of the confined region is 92.8%. In spite of this large relative error, the total quadrature error is small since the energy contribution of the confined region to the energy stored in the cross-section is only 2.5%.

Although the present transverse Gauss rule in SINGER appears to be adequate, the user has no means of estimating or controlling the resulting errors. Hence, it is strongly recommended that a variable transverse Gauss rule be introduced in SINGER.

ERROR CONTROLS

It is recommended that the initial selection of the finite element mesh of the structure and the Gauss rule of each element be based on a preliminary analysis of the "test problem". The cross-sectional properties of the test problem should correspond to those of the actual structure (this may require several test problems for one structure). The objective of the preliminary analysis is to determine the length and the Gauss rule of the finite element for each range of response (e.g., elastic range, hinge element) that will

keep the discretization and quadrature errors within specified bounds.

The computation of the exact value of the extreme fiber strain in compression at the fixed end can be performed via classical methods or directly with SINGER. Since the stress resultant at the fixed end is known, the strain state (in the elastic and inelastic range) can be found from conditions of equilibrium. In the inelastic range an iterative approach is necessary if the strain state is sought for a prescribed moment. On the other hand, one can prescribe the strain state and compute the corresponding moment directly (analogous to the approach used to generate interaction diagrams for reinforced concrete columns). Alternatively, the strain state at the fixed end can be computed with SINGER to any desired degree of accuracy by selecting the element length sufficiently small.

SECTION V

NEW FINITE ELEMENT MODEL

In order to minimize the directional preference (section II) and improve the accuracy (section IV) of the finite element model in SINGER, a new model has been developed. It differs from the old model as follows:

1. The x-axis of the local moving frame reference is collinear with chord that joins the two external nodes of the element, and the origin of the reference frame coincides with the midpoint of the chord (fig. 7).
2. The strain field is described by a polynomial of order 1 in both local coordinates; i.e., the strain field is linear.

COORDINATE TRANSFORMATION

The transformation of the global nodal displacements into local deformation components follows from figure 7:

$$\bar{u}_1 = \Delta/2 \tag{30}$$

$$\bar{u}_2 = U_{i3} - \gamma \tag{31}$$

$$\bar{u}_3 = U_{j3} - \gamma \tag{32}$$

where

$$\gamma = \beta - \alpha \tag{33}$$

$$\Delta = |\Delta X^*| - |\Delta X| \tag{34}$$

$$|\Delta X^*| = [(\Delta X_1^*)^2 + (\Delta X_2^*)^2]^{1/2} \tag{35}$$

$$|\Delta X| = [(\Delta X_1)^2 + (\Delta X_2)^2]^{1/2} = L \tag{36}$$

$$\Delta X = X_j - X_i \tag{37}$$

$$\Delta X^* = \Delta X + \Delta U \tag{38}$$

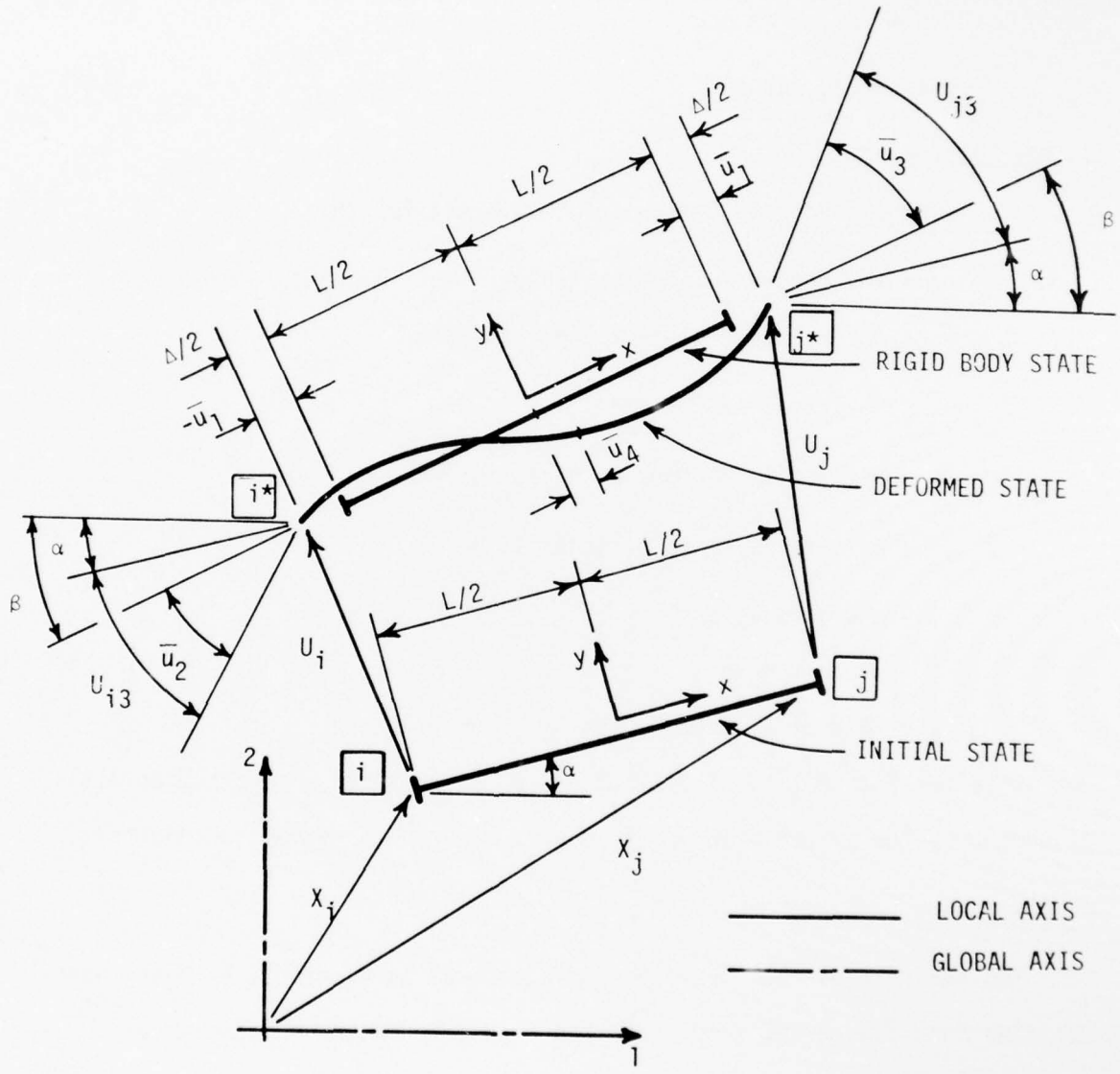

FIG. 7 COORDINATE TRANSFORMATION

$$\Delta U = U_j - U_i \tag{39}$$

$$\gamma = \tan^{-1}(a/b) \tag{40}$$

$$a = \Delta X_1 \Delta X_2^* - \Delta X_1^* \Delta X_2 \tag{41}$$

$$b = \Delta X_1^* \Delta X_1 + \Delta X_2^* \Delta X_2 \tag{42}$$

In Eqs. 30 thru 42

$\bar{u}_1$ = one half of the change in element length

Δ = the change in element length

$\bar{u}_2, \bar{u}_3$ = the relative element end-rotations

U_{i3}, U_{j3} = rotations of the nodes i, j

U_i, U_j = deflection vectors of nodes i, j

X_i, X_j = position vectors of nodes i, j

γ = chord rotation

$|X^*|$ = chord length

L = initial element length

Note that the internal nodal deflection, $\bar{u}_4$, represents a generalized displacement of the system model [1]; hence, no transformation is required.

FINITE ELEMENT MODEL

The deformation field of the discrete model is described by four interpolation functions corresponding to the four deformation components $\bar{u}_1$, $\bar{u}_2$, $\bar{u}_3$, and $\bar{u}_4$ (figure 7). The interpolation functions are expressed in terms of the normalized coordinate

$$t = \frac{2}{L}x, \quad -1 \leq t \leq 1 \tag{43}$$

AXIAL INTERPOLATION

On the basis of the Lagrange interpolation formula [24], the axial deflection, u, can be expressed as

$$u = \ell_1 u(-1) + \ell_2 u(o) + \ell_3 u(1) \tag{44}$$

where

$$\ell_1 = t(t-1)/2 \tag{45}$$

$$\ell_2 = (1+t)\ (1-t) \tag{46}$$

$$\ell_3 = t(t+1)/2 \tag{47}$$

Imposing the continuity conditions (figure 7)

$$-u(-1) = u(1) = \bar{u}_1 \tag{48}$$

$$u(o) = \bar{u}_4 \tag{49}$$

one obtains

$$u = \Phi_1 \bar{u}_1 + \Phi_4 \bar{u}_4 \tag{50}$$

where

$$\Phi_1 = t$$

$$\Phi_4 = (1-t^2) \tag{52}$$

TRANSVERSE INTERPOLATION

With the aid of the Hermite interpolation formula [24], the transverse deflection, v, can be expressed as

$$v = \Phi_2 q_2 + \Phi_3 q_3 \tag{53}$$

where

$$q_2 = \bar{u}_2 L/2 \tag{54}$$

$$q_3 = \bar{u}_3 L/2 \tag{55}$$

$$\Phi_2 = (t+1)(t-1)^2/4 \tag{56}$$

$$\Phi_3 = (t-1)(t+1)^2/4 \tag{57}$$

Note that

$$\frac{dv}{dx} = \Phi_2'\bar{u}_2 + \Phi_3'\bar{u}_3 \tag{58}$$

where

$$\Phi_2' = (t-1)(3t+1)/4 \tag{59}$$

$$\Phi_3' = (t+1)(3t-1)/4 \tag{60}$$

It follows that v satisfies the boundary conditions (figure 7)

$$v(-1) = v(1) = 0 \tag{61}$$

$$\frac{dv}{dx}(-1) = \bar{u}_2 \tag{62}$$

$$\frac{dv}{dx}(1) = \bar{u}_3 \tag{63}$$

STRAIN FIELD

The strain-displacement relation of the beam-column can be expressed in the form [1]

$$\varepsilon(x,y) = \frac{du}{dx} + \frac{1}{2}\left(\frac{dv}{dx}\right)^2 - y\frac{d^2v}{dx^2} \tag{64}$$

or

$$\varepsilon(t,s) = \frac{2}{L}\frac{du}{dt} + \frac{2}{L^2}\left(\frac{dv}{dt}\right)^2 - \frac{4s}{L}\frac{d^2v}{dt^2} \tag{65}$$

where

$$s = y/L \tag{66}$$

When u and v are discretized according to Eqs. 50 and 53, the first and third term on the right-hand side of Eq. 65 become polynomials in t of order 1

while the second term (the coupling term) becomes a polynomial in t of order 4. As discussed in section IV, a prerequisite for ε to vanish identically along the reference axis (i.e., for $\varepsilon(t,o) \equiv 0$) is that the polynomials of the first and second term of Eq. 65 are of the same order. This condition can be satisfied without increasing the degrees of freedom of the element by decreasing the order of the polynomial of the second term from 4 to 1. Accordingly, let

$$\varepsilon(t,o) = \frac{2}{L}\frac{du}{dt} + \frac{2}{L^2}\left(\frac{dv}{dt}\right)^2 = a_o + a_1 t \tag{67}$$

where a_o, a_1 are undetermined coefficients. The solution to Eq. 67 can be expressed in the form

$$\frac{2}{L}[u(t)-u(-1)] = \int_{-1}^{t} (a_o + a_1 t)dt - \frac{2}{L^2}\int_{-1}^{t} \left(\frac{dv}{dt}\right)^2 dt \tag{68}$$

Integration of Eq. 68 and substitution of the continuity conditions, Eqs. 48, 49, into Eq. 68 yields two algebraic equations in the unknown coefficients:

$$\frac{2}{L}(\bar{u}_1 + \bar{u}_4) = a_o - \frac{1}{2}a_1 - 2B \tag{69}$$

$$\frac{4}{L}\bar{u}_1 = 2a_o - 2A \tag{70}$$

where

$$A = \frac{1}{L^2}\int_{-1}^{1} \left(\frac{dv}{dt}\right)^2 dt \tag{71}$$

and

$$B = \frac{1}{L^2}\int_{-1}^{0} \left(\frac{dv}{dt}\right)^2 dt \tag{72}$$

The solution of Eqs. 69, 70 yields

$$a_o = \frac{2}{L}\bar{u}_1 + A \tag{73}$$

$$a_1 = \frac{-4}{L}\bar{u}_4 + 2(A-2B) \tag{74}$$

and from Eqs. 67, 73 and 74 one obtains

$$\varepsilon(t,o) = \frac{2}{L}(\bar{u}_1 - 2t\bar{u}_4) + (\alpha + \beta t) \tag{75}$$

where

$$\alpha = A \tag{76}$$

$$\beta = 2(A-2B) \tag{77}$$

Note that the first term on the right-hand side of Eq. 75 can be obtained by substituting Eq. 50 into Eq. 67; hence, the second term of Eq. 75 represents the linearized coupling term. Substitution of Eq. 53 into Eqs. 71, 72 and integration yields A and B, which can be substituted into Eqs. 76, 77 to yield

$$\alpha = \frac{1}{15}(\bar{u}_2^2 - \frac{1}{2}\bar{u}_2\bar{u}_3 + \bar{u}_3^2) \tag{78}$$

$$\beta = \frac{1}{16}(\bar{u}_3^2 - \bar{u}_2^2) \tag{79}$$

Observe that Eq. 65 can be expressed as

$$\varepsilon(t,s) = \varepsilon(t,o) - \frac{4s}{L}\frac{d^2v}{dt^2} \tag{80}$$

Substitution of Eq. 53 into Eq. 80 yields

$$\varepsilon(t,s) = \varepsilon(t,o) - s[(3t-1)\bar{u}_2 + (3t+1)\bar{u}_3] \tag{81}$$

Finally, on the basis of Eqs. 75 and 81, one can express the strain field of the new finite element model in the form

$$\varepsilon(t,s) = (\frac{2}{L}\bar{u}_1+\alpha) + (\beta-\frac{4}{L}\bar{u}_4)t - s[(3t-1)\bar{u}_2 + (3t+1)\bar{u}_3] \qquad (82)$$

which represents a complete polynomial in t and s of order 1.

SECTION VI

CAPABILITY OF SINGER

The SINGER program was designed to predict the response of skeletal structural systems incorporating nonlinear material characteristics as well as finite displacement configurations. The system inertia forces included in the solution process provide a dynamic capability. This section is intended to demonstrate the analysis capability of the current version of the program by studying the type of problems that can be analyzed as well as the accuracy of the macro response predictions. In addition, the convergence characteristics of certain strain discontinuities are documented. In each problem, the behavior is intended to represent the entire continuum range up to the ultimate state. This is insured by supressing the local element failure checks associated with the failure criteria developed earlier.

DEMONSTRATION PROBLEMS

The demonstration problems documented are primarily concerned with the static response predictions of reinforced concrete systems. The two dynamic problems are single degree of freedom systems; one problem has an elastoplastic material, while the other problem has reinforced concrete properties. Each problem is developed to include the description of the system, materials, and the time dependent forcing function if appropriate. The computed response is shown in comparison with some reference response data.

PROBLEM NO. 1: REINFORCED CONCRETE BEAM

The system analyzed in this problem is a simply supported

reinforced concrete beam with a concentrated transverse load applied at the center of the span. The results demonstrate the static prediction capability for a reinforced concrete system gradually loaded to failure. The comparison basis is the experimental test results of the corresponding physical beam measured by the load-deflection function to failure published by Burns and Siess [25]. Figure 8 shows the system details and the material properties; figure 9 shows the load-deflection response comparison between the computed and experimental values.

The comparison shows only small differences between the two functions up to the limit point. The largest deviations occur near the yield load level, but limit point is accurately predicted.

PROBLEM NO. 2: CERF BEAM TEST

This system is a simply supported reinforced concrete beam with two equal lateral forces applied symmetrically with respect to the center of the span. The predicted response is intended for comparison with specific experimental results obtained for beam 5-0-1 at the Civil Engineering Research Facility [26].

The geometry of the beam is shown in figure 10. The beam was divided into 12 elements, two of which were steel end plates which were used for loading the beam in the test apparatus. The remaining 10 elements had cross sections as shown. The beam element nodes were selected to correspond to instrumentation locations of the experimental test beams. The material properties of the concrete and steel were chosen to match the experimental properties; these are shown in figure 11. The equal lateral loads, F/2, were located at nodes 6 and 8.

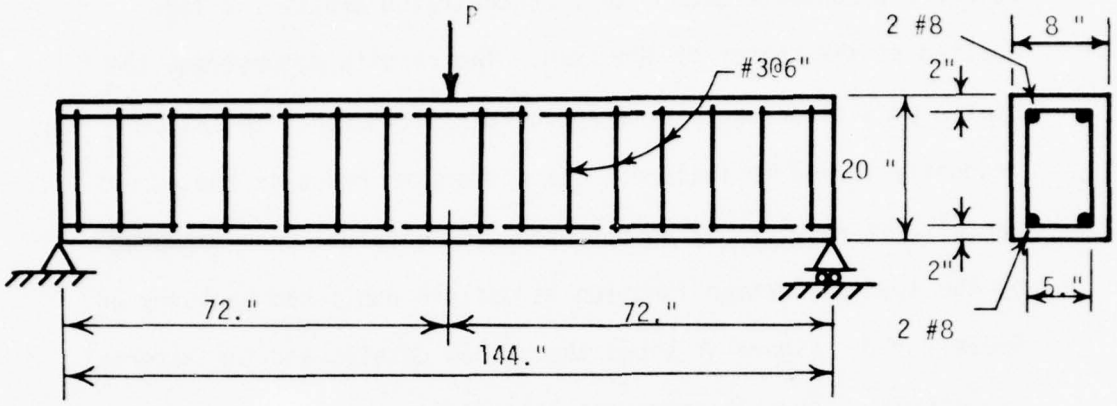

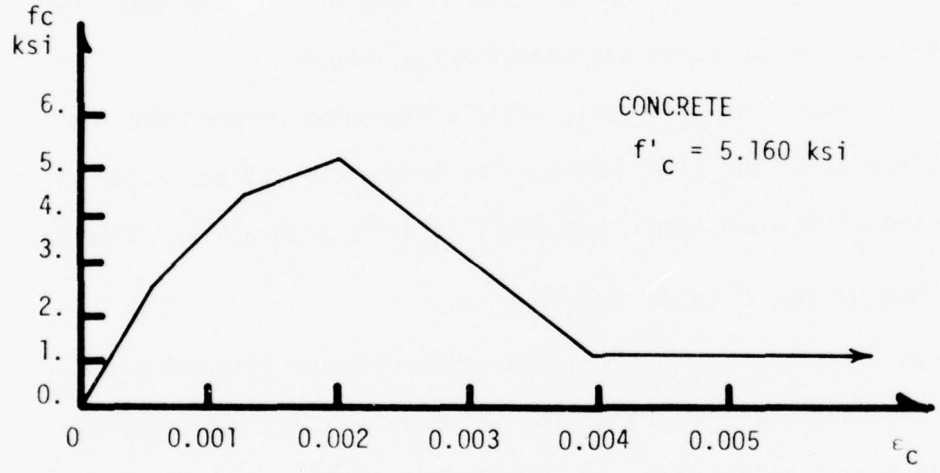

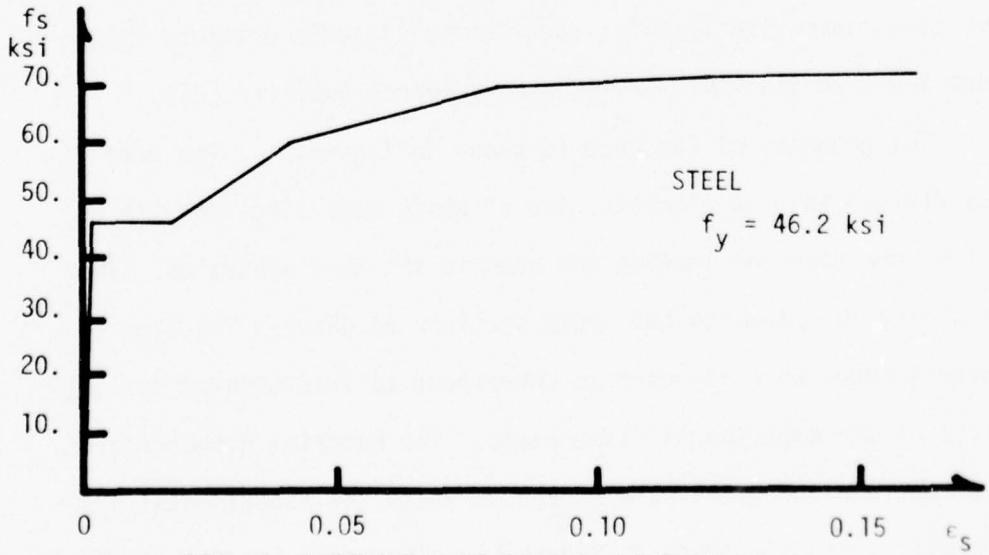

FIG. 8 SYSTEM AND MATERIALS, PROBLEM NO. 1

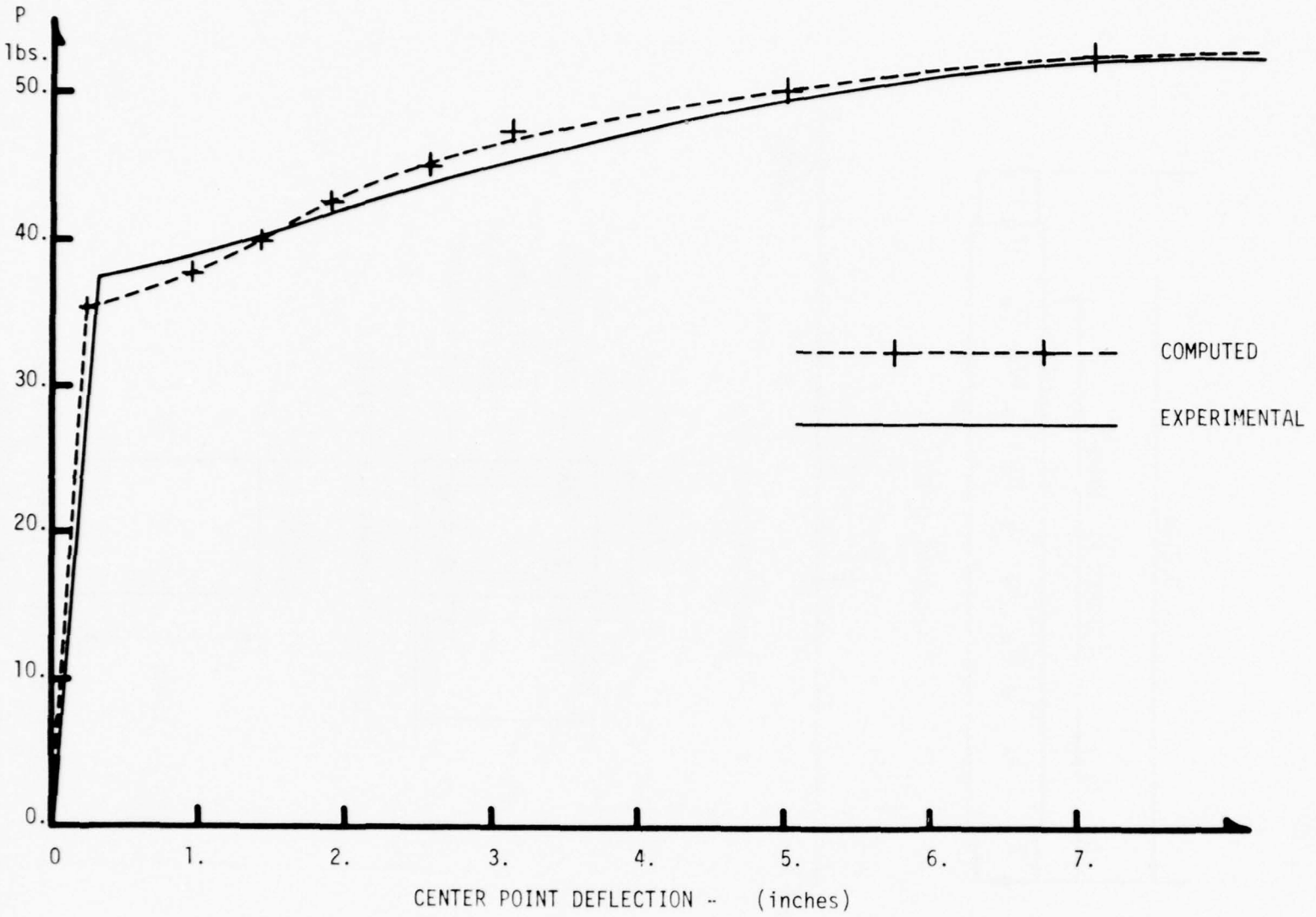

FIG. 9 RESPONSE COMPARISON, PROBLEM NO. 1

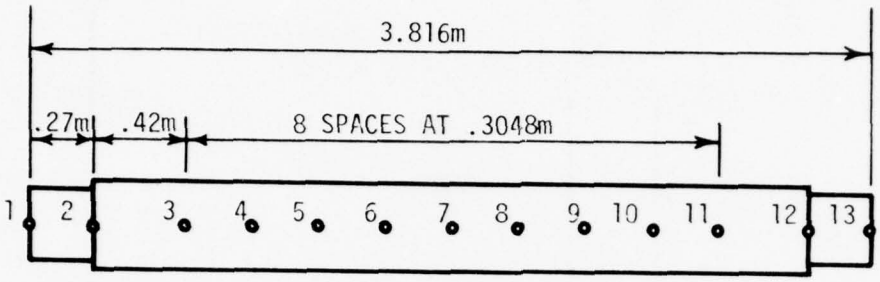

LOCATION OF NODES

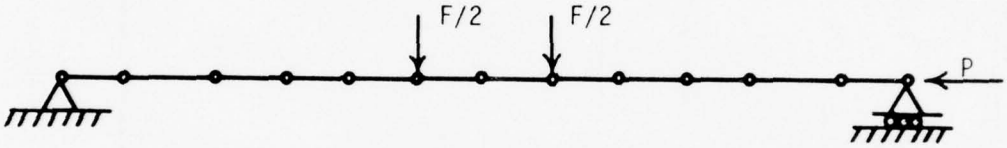

LOADED REFERENCE AXIS

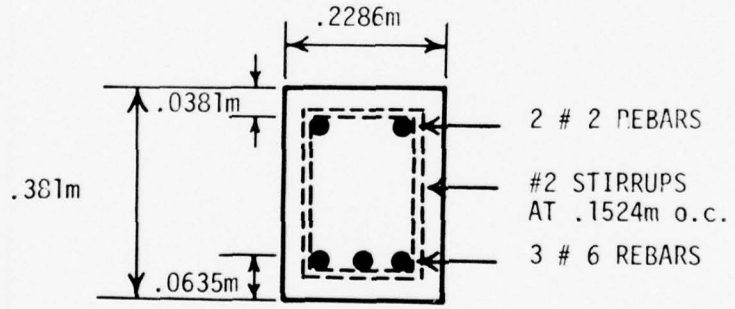

SECTION, ELEMENTS 2-3 TO 11-12

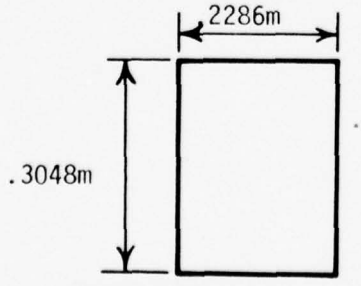

STEEL SECTIONS, ELEMENTS 1-2 & 12-13

FIG. 10 UNM/CERF BEAM-COLUMN, PROBLEM NO. 2

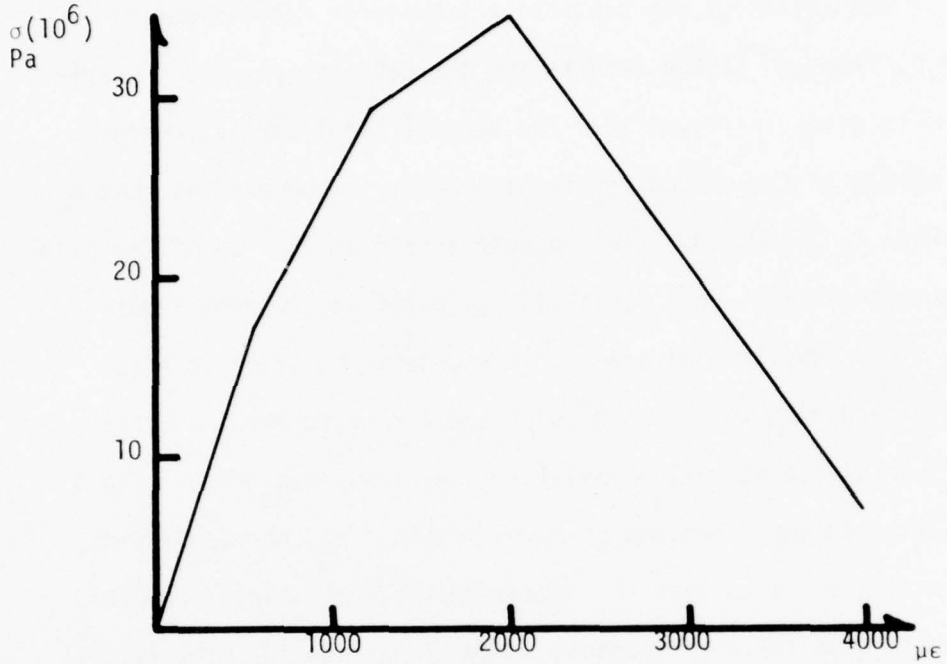

CONCRETE STRESS-STRAIN

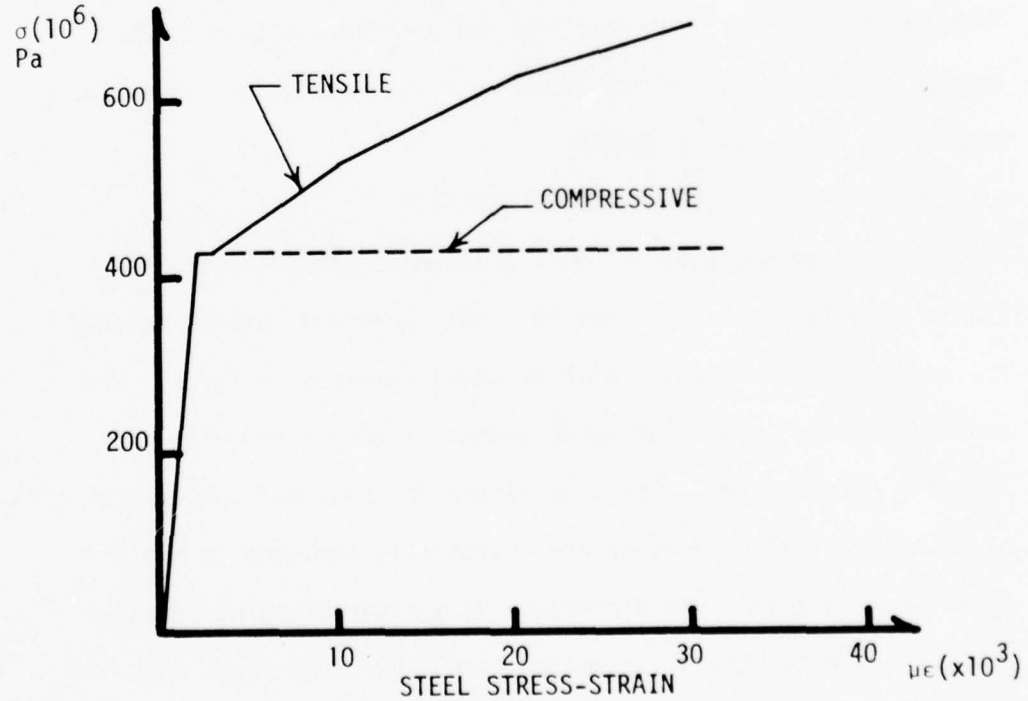

STEEL STRESS-STRAIN

FIG. 11 MATERIAL PROPERTIES, PROBLEM NO. 2

A comparison of the centerline transverse displacements, node 7, from the SINGER results and the CERF experimental measurements is given in figure 12. The tensile steel strain, which is the strain in the bottom reinforcing bars, is compared at node 6 as shown in figure 13. The concrete strain at the top of the beam at the centerline, node 7, is also compared in the same figure.

These results indicate that the general behavior is accurately predicted for both the displacement measurement and the strain measurement well beyond the linear response range. The results also show that the computed response has more stiffness in the linear range than the corresponding experimental results. However, when the displacements become large and the beam is well within the inelastic region of response, SINGER exhibits less stiffness than the experimental behavior. The SINGER program terminated execution when the load was incremented beyond the maximum load capacity of the beam. Collapse conditions were not accurately predicted by SINGER.

PROBLEM NO. 3: CERF BEAM-COLUMN TEST

The system analyzed for this problem is identical to the system details shown in figure 10. The two equal lateral forces are applied in combination with an axial compressive force. The static response prediction is intended for comparison with the specific experimental results developed for beam 5-2-1 from CERF [26].

The material properties are essentially the same as those shown in figure 11. One difference is a lower crushing strength for the concrete stress-strain function. For this beam, the crushing strength was approximately 4336. psi (29.9 MPa). The

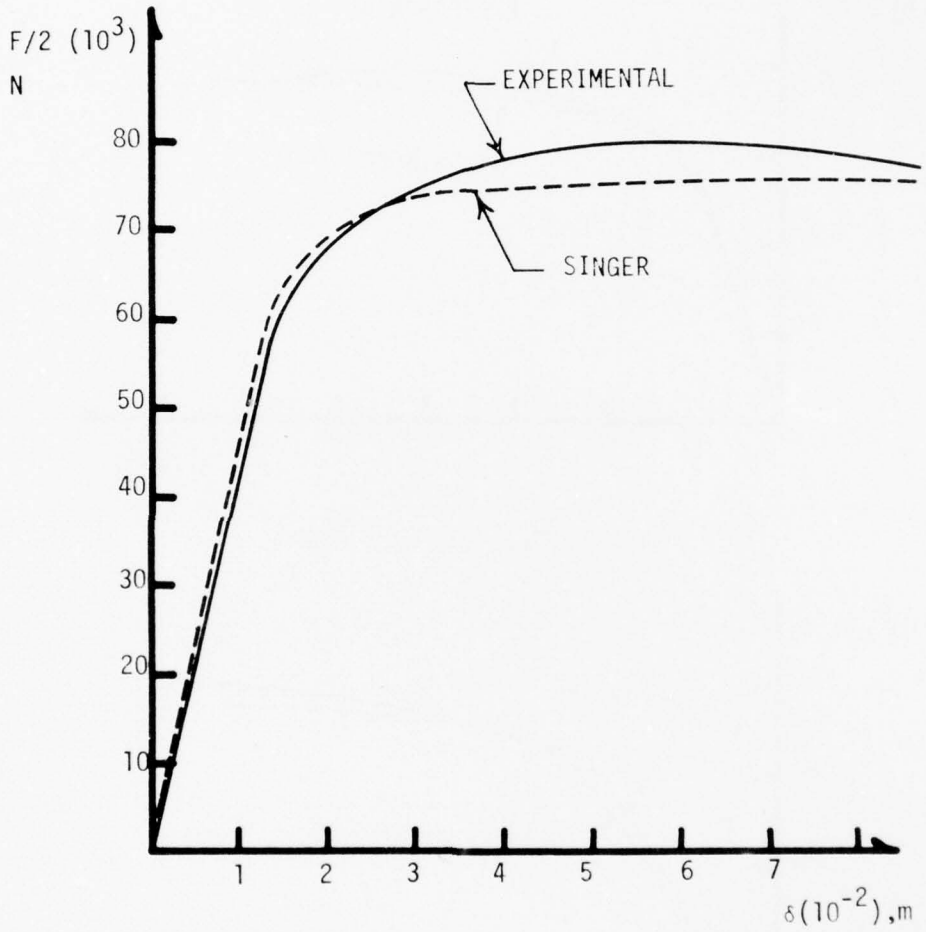

FIG. 12 CENTERLINE DISPLACEMENT OF CERF BEAM 5-Ø-1, PROBLEM NO. 2

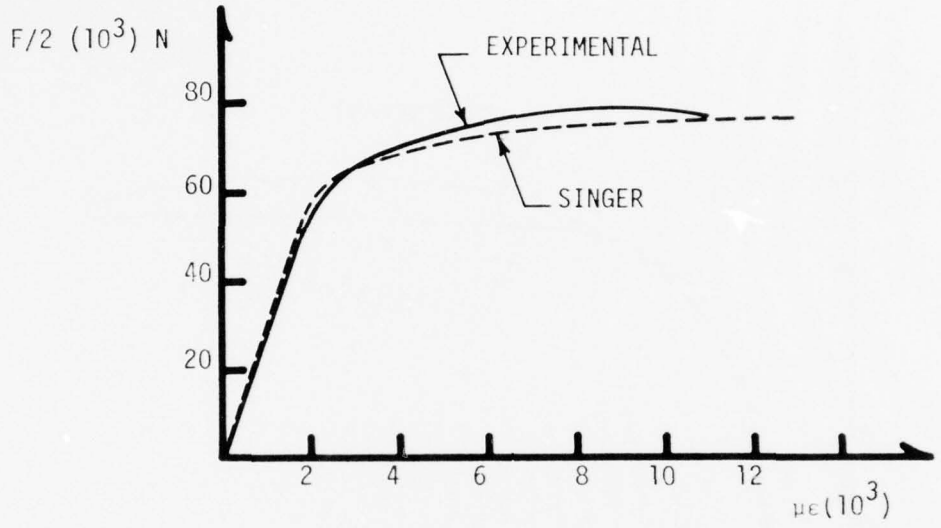

TENSILE STEEL STRAIN, NODE 6

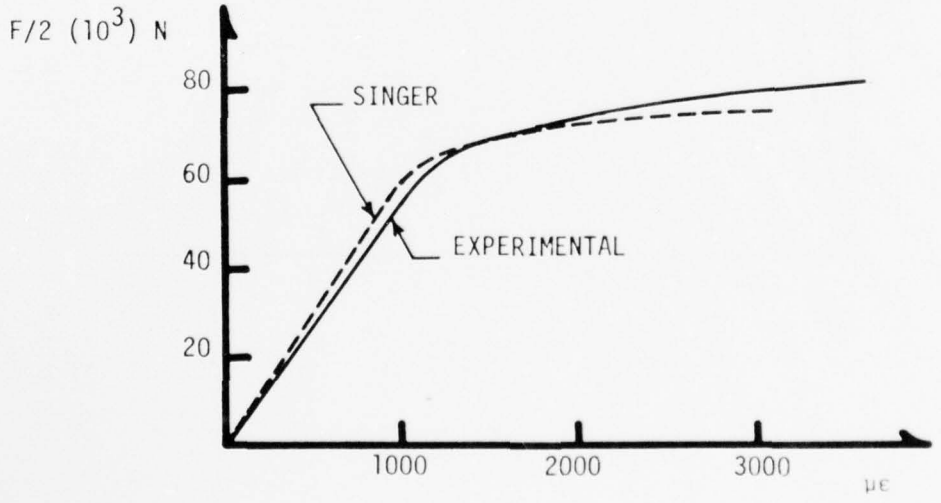

TOP FIBER CONCRETE STRAIN, NODE 7

FIG. 13 BEAM 5-0-1 STRAIN COMPARISONS, PROBLEM NO. 2

loading consisted of the two lateral forces F/2 and the combined axial force P. The ratio P/F of 1.91 was developed for each load increment to failure.

The response comparison is based on displacement and strain measurements. The centerline displacement, node 7, for both SINGER and the experimental test measurements is given in figure 14. A comparison of the tensile strains in the bottom reinforcing steel at node 6 is shown in figure 15. The concrete strain at the top of the beam at the centerline (node 7) is also illustrated in figure 15. The computed results accurately predict the initial response and the limit point but fail to define the gradual loss of stiffness near the yield load. The decreasing experimental load-deflection path beyond the limit point cannot be developed by the program since the equilibrium path beyond the limit state is unstable. Experimentally, this region of the function can be defined since the displacements can be physically controlled and the forces adjusted accordingly. Comparison of centerline displacement quantities of beam 5-2-1 indicates that the finite element model of SINGER is stiffer than the experimental beam all the way to collapse. The tensile steel strain comparison reflects this behavior. This demonstrates that the steel response may dominate the system response.

PROBLEM NO. 4: REINFORCED CONCRETE WITH CYCLIC AXIAL LOAD

The system analyzed is a reinforced concrete member with a force applied parallel to the longitudinal axis. The force is first incremented as a compression force up to the value of

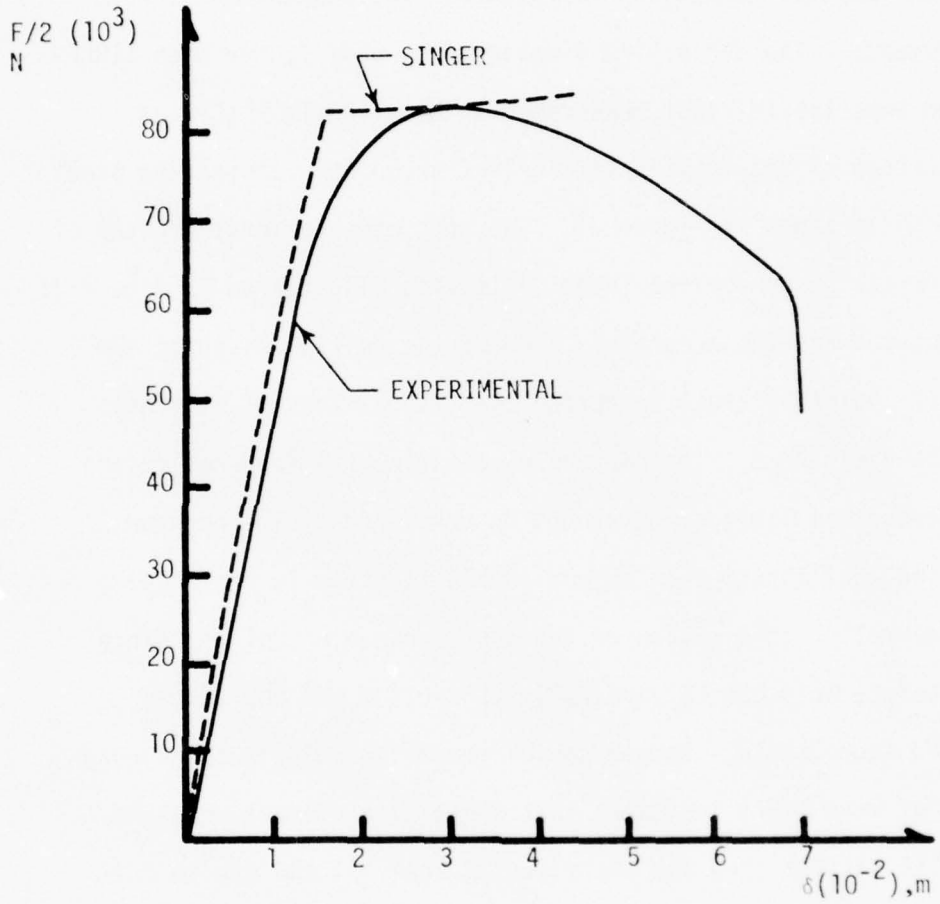

FIG. 14 CENTERLINE DISPLACEMENT OF CERF BEAM 5-2-1, PROBLEM NO. 3

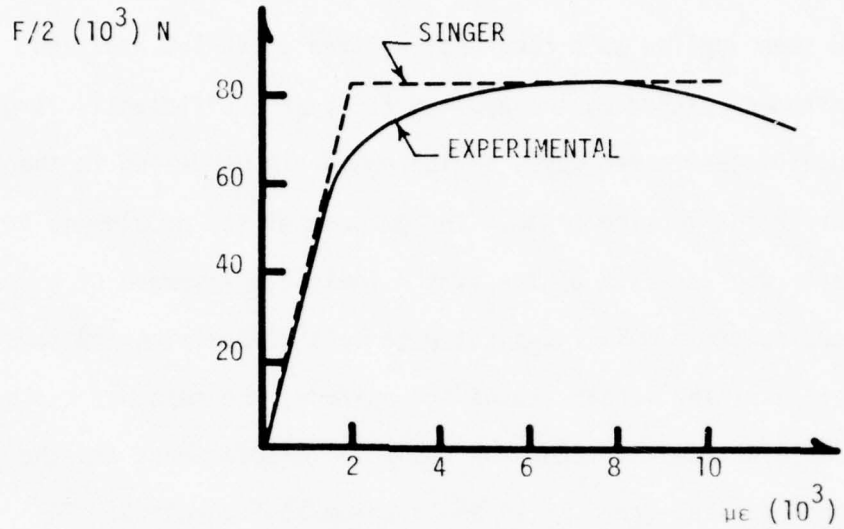

TENSILE STEEL STRAIN, NODE 6

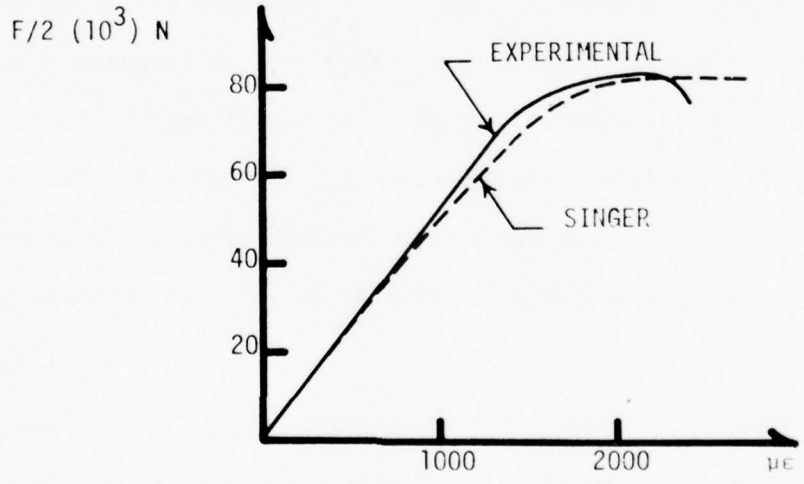

TOP FIBER CONCRETE STRAIN, NODE 7

FIG. 15 BEAM 5-2-1 STRAIN COMPARISONS, PROBLEM NO. 3

650.X10^3 lbs. so that both the steel and concrete are active. From this point, the force is reduced to zero, then applied as a tension force up to 150.X10^3 lbs. At this value it is again reduced to zero and then applied as a compression force up to 150.X10^3 lbs. The magnitudes reached by the applied force are sufficiently large to produce inelastic response, including strain hardening in the steel during the tension range. The purpose of the problem is to demonstrate the accuracy of the static inelastic response of a reinforced concrete member subjected to both compression and tension. Since the resulting strain states are uniform, the response can be checked by exact calculations for the axial displacement and the corresponding axial force at an equilibrium configuration. The system and materials used are shown in figure 16; the response and comparison checks are shown in figure 17. The check values agree perfectly with the computed response. Very good convergence characteristics are usually obtained for the solution of axially loaded systems for the complete range of response. The large displacement values in the tension range are due to the lack of concrete strength in tension. The tensile force is resisted only by the reinforcing bars.

PROBLEM NO. 5: SINGLE DEGREE OF FREEDOM ELASTIC-PLASTIC SPRING

This system consists of an ideal massless spring (bar) with mass attached at the free end. A time-dependent forcing function is applied to the mass in the axial direction so that the resulting system has only a single degree of freedom. The material has ideally elastic-plastic properties with a linear unloading

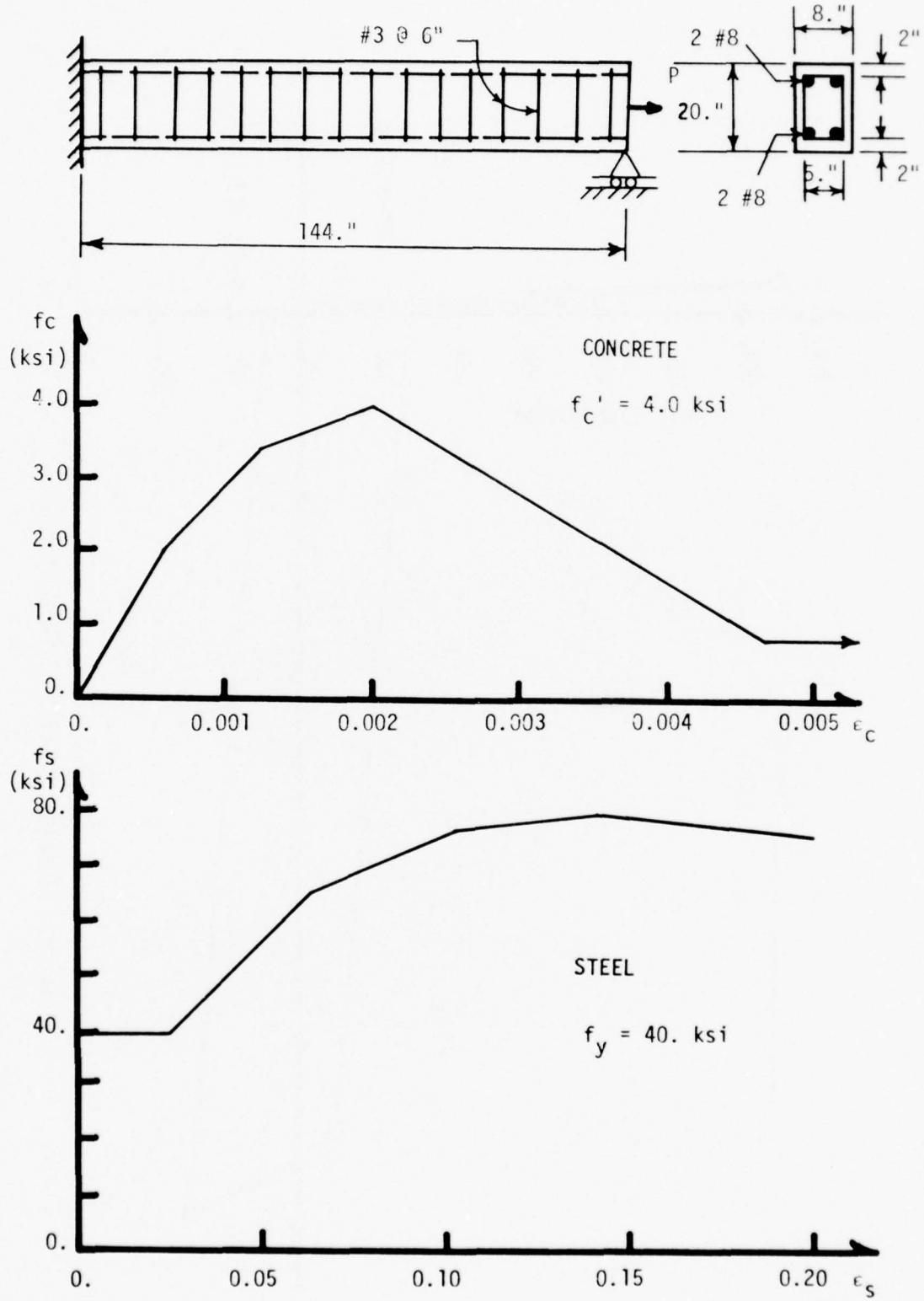

FIG. 16 SYSTEM AND MATERIALS, PROBLEM NO. 4

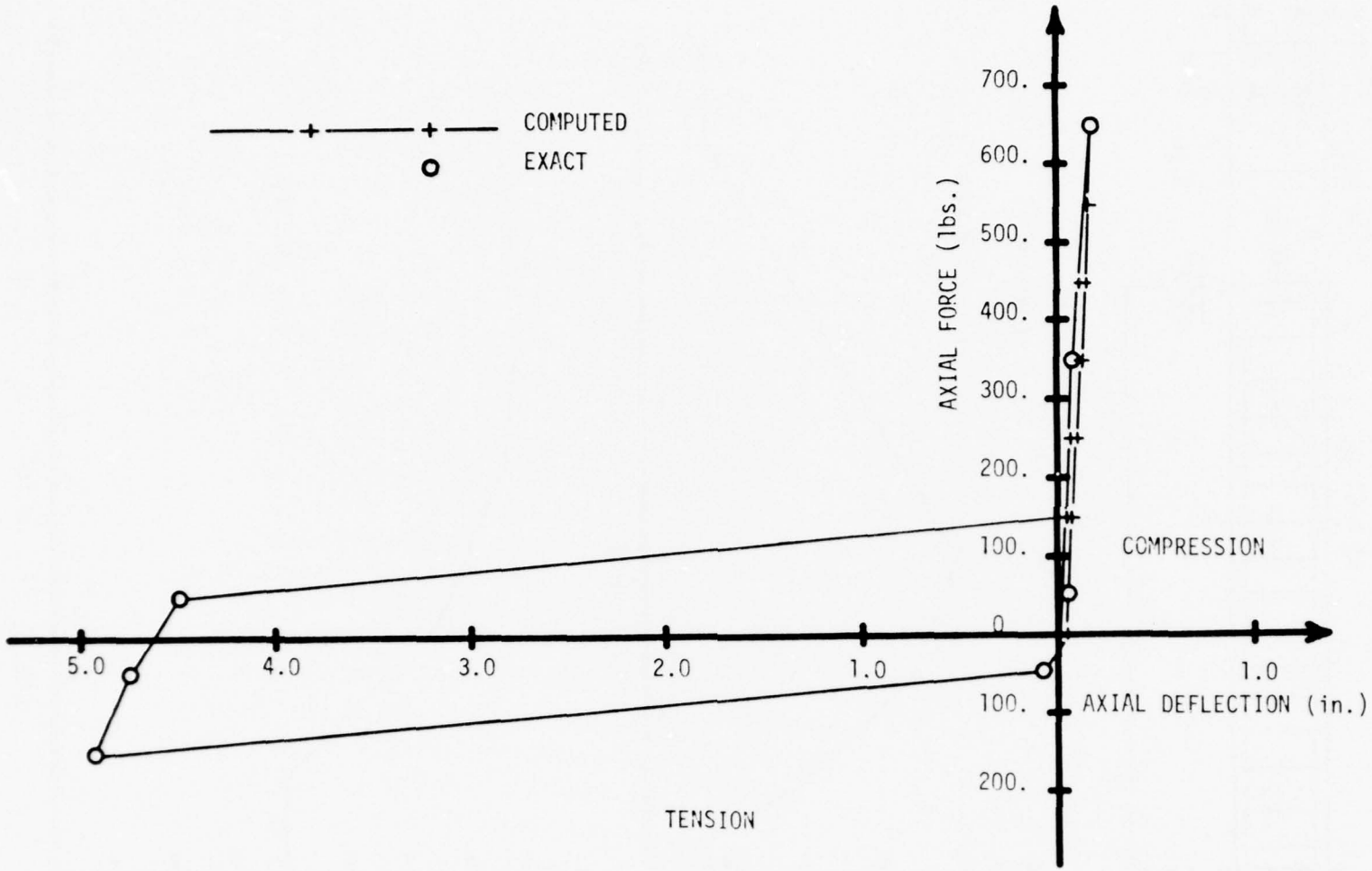

FIG. 17 RESPONSE COMPARISON, PROBLEM NO. 4

charateristic; the forcing function is a decreasing triangular pulse. The system, material function, and forcing function are shown in figure 18.

The purpose is to demonstrate the dynamic capability with inelastic response using a problem which can be checked by exact computations. The displacement response and comparison checks are shown in figure 19. Although the computed and exact functions are almost identical in the initial portion of the response, accumulated errors eventually cause some discrepancy to appear and grow. The error observed in this problem is primarily a phase shift in the displacement function.

PROBLEM NO. 6: REINFORCED CONCRETE BEAM WITH AXIAL FORCE PULSE

This problem analysis develops the response for a massless reinforced concrete element with attached mass at the free end. The single degree of freedom system has an applied force pulse in the axial direction. The material properties are linearized so that a closed form solution can be used as a comparison basis. The element details and the forcing function are shown in figure 20.

Both concrete and steel properties are defined in terms of their respective modulus of elasticity. For concrete, the elastic modulus is 34.474 GPa , while the steel modulus is 241.315 GPa The forcing function is a linearly decreasing triangular force pulse which varies from 650 kN at time zero to a zero value at time 0.002 second .

The closed form displacement response during the loading phase is

$$U(t) = P_o/k(\sin(\omega t)/\omega t_1 - \cos(\omega t) - t/t_1 + 1)$$

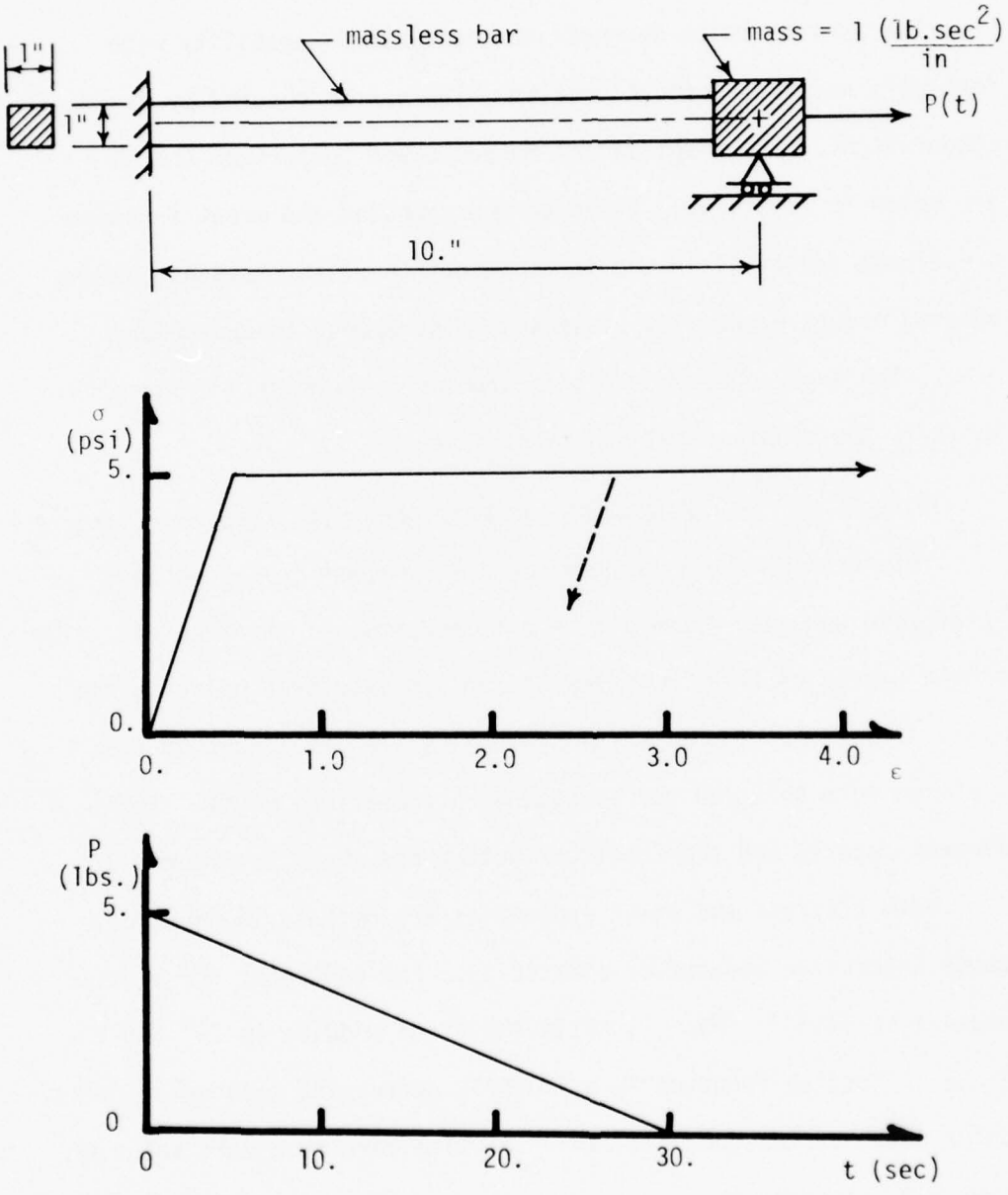

FIG. 18 SYSTEM, MATERIAL, AND FORCING FUNCTION, PROBLEM NO. 5

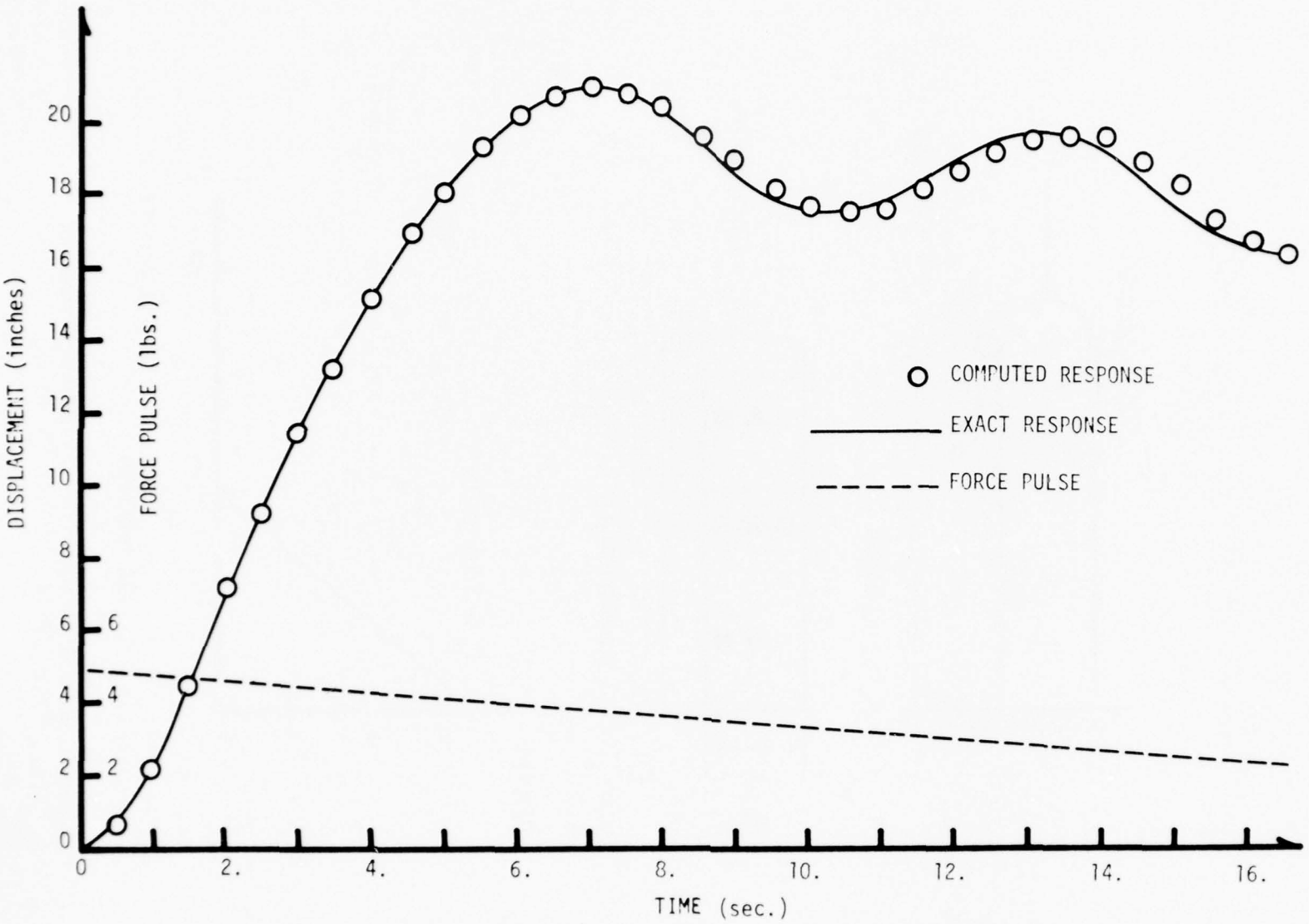

FIG. 19 DISPLACEMENT - TIME RESPONSE COMPARISON, PROBLEM NO. 5

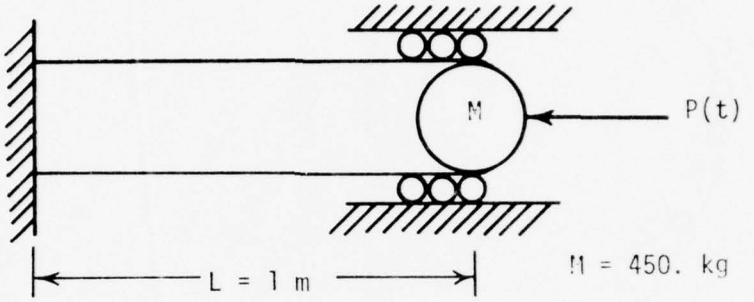

LOADED BEAM

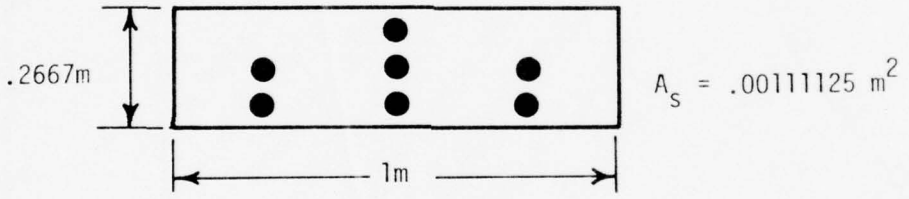

CROSS-SECTION

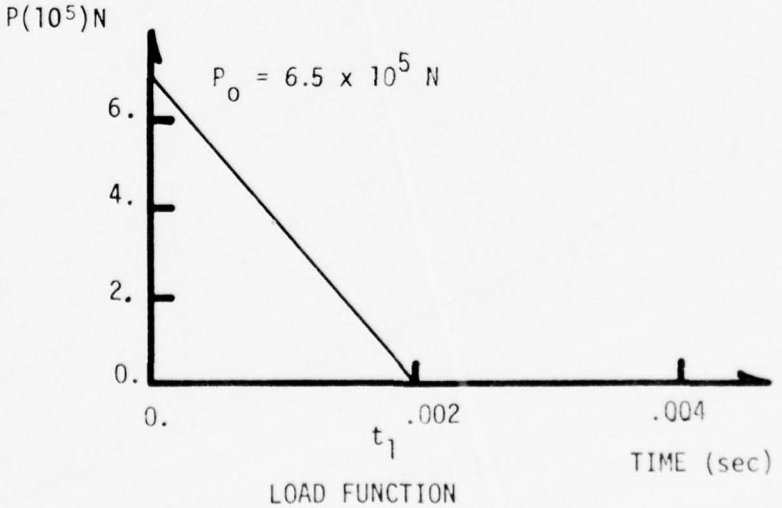

LOAD FUNCTION

FIG. 20 REINFORCED CONCRETE BEAM WITH A TRIANGULAR PULSE LOADING, PROBLEM NO. 6

where k is the stiffness defined as AE/L; A is the transformed cross-sectional area of concrete, E is the elastic modulus of concrete and L is the length of the element. The natural frequency, ω is defined as $\sqrt{(k/M}$, where M is the concentrated x-component of mass. The constant t_1 is the time at which the force has decreased to zero, 0.002 second.

Comparison of the SINGER response with the theoretical response is shown in figures 21 and 22. The comparison is only made through the point where the beam is still in compression. The closed form solution would have to be re-evaluated for the response when tension occurs since the stiffness will be changed. For the time of response that is compared, there is negligible difference between the SINGER prediction and the closed form solution. When the beam goes into tension, the response time increases indicative of the longer period.

CONVERGENCE CHARACTERISTICS OF STRAIN DISCONTINUITY

It has been observed in computed output that a single element required to represent relatively large changes in strain within its length may in fact create a strain discontinuity with respect to an adjacent element while achieving a system equilibrium configuration. Large changes in strain within an element occur when one element is severely strained beyond the yield state of the material while an adjacent element is much less severely yielded, or it is not yielded at all. The strain values at the sections on either side of a connecting joint may differ not only in magnitude but also in sign. This discontinuous behavior has been observed in computed results for reinforced concrete elements as well as for steel wide flange elements. The number of elements

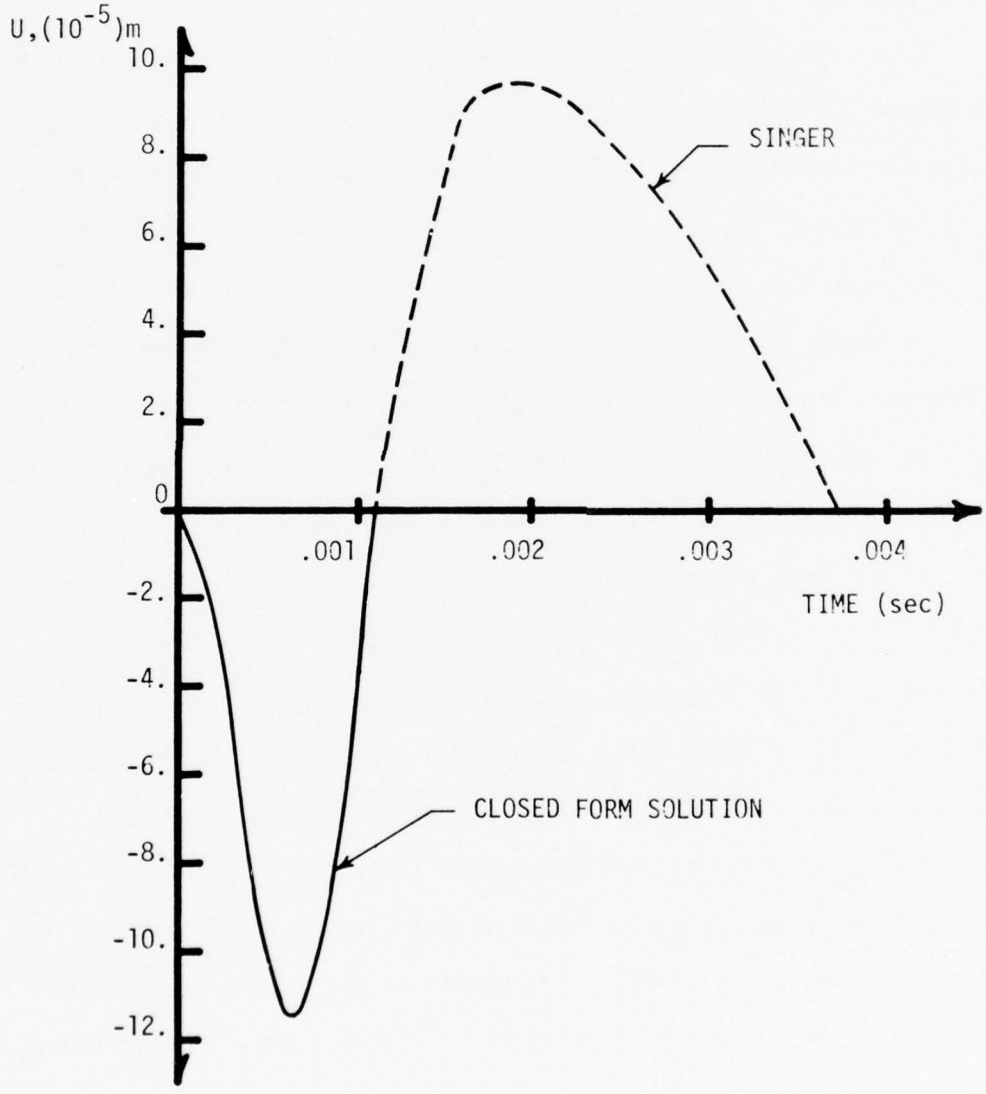

FIG. 21 COMPARISON OF DISPLACEMENT RESPONSE TO AN IMPULSE LOAD, PROBLEM NO. 6

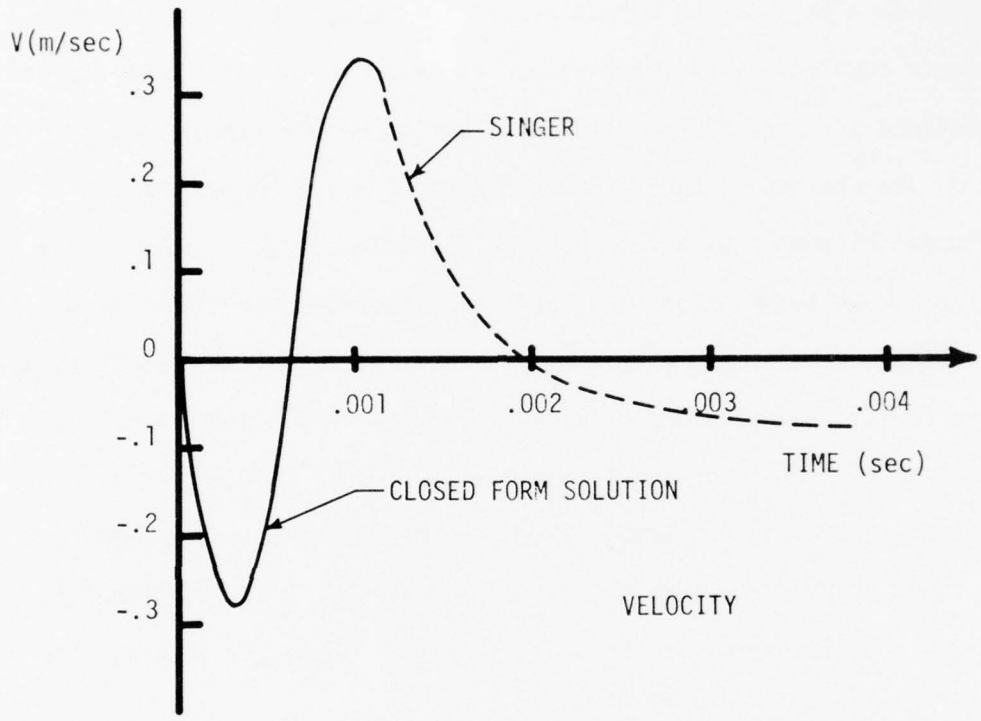

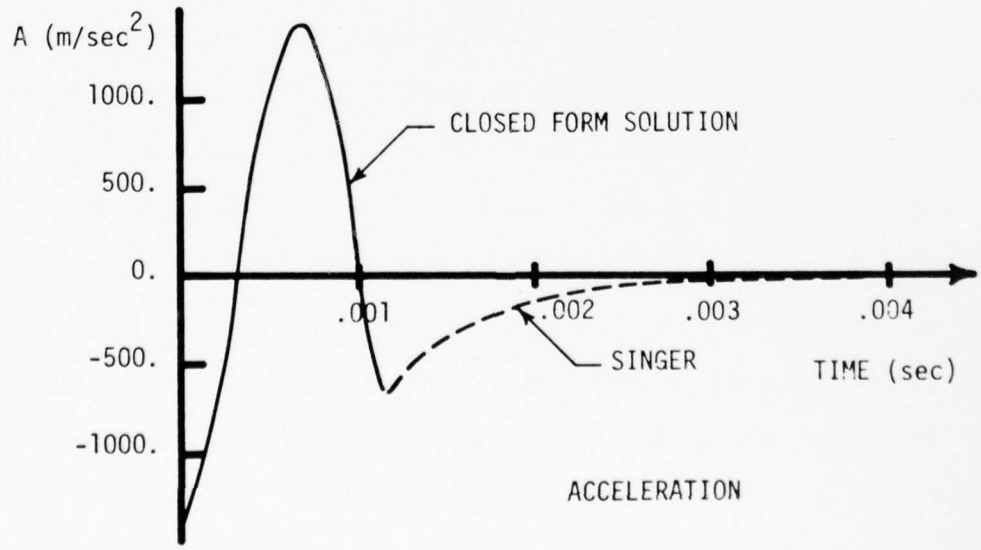

FIG. 22 COMPARISON OF VELOCITY AND ACCELERATION OF CONCRETE BEAM, PROBLEM NO. 6

chosen to represent the system can significantly affect the form and severity of the discontinuities created. The strain values which occur as a part of the output record for measuring the interelement strain continuity are those values computed at the points of the end sections of each element after equilibrium has been achieved.

The characteristics of strain discontinuity are documented in figures 23 and 24 with the specific objective to show the relative strain magnitudes which occur and to demonstrate the effect of increasing the number of elements. The problem data are identical to the data for problem No. 1 (figure 8) with slight differences in the material properties: f'_c = 4000. psi and f_y = 40,000. psi. The strain in the tension steel is used to measure the strain behavior. Figure 23 shows the strain distribution at the first load level to cause the discontinuous behavior; figure 24 shows the distribution at the next load increment.

In a reinforced concrete section, the tension requirement for bending is satisfied by the reinforcing steel only; in SINGER, the concrete material has no tensile strength. The effect of this property is that once the steel begins to yield, the strain passes almost immediately into the strain hardening range since there is no other source of positive stiffness to resist increased loads. The strain is, therefore, either below the yield strain or into the strain hardening region. This severe strain gradient near the section of maximum bending moment corresponds to large deformation changes in a highly localized region of the beam. As shown in figure 23, the strains change from yield strain (0.00138) to the order of twice strain hardening (0.023) within a distance of 0.9 times the depth of the beam. In figure 24, the next higher load

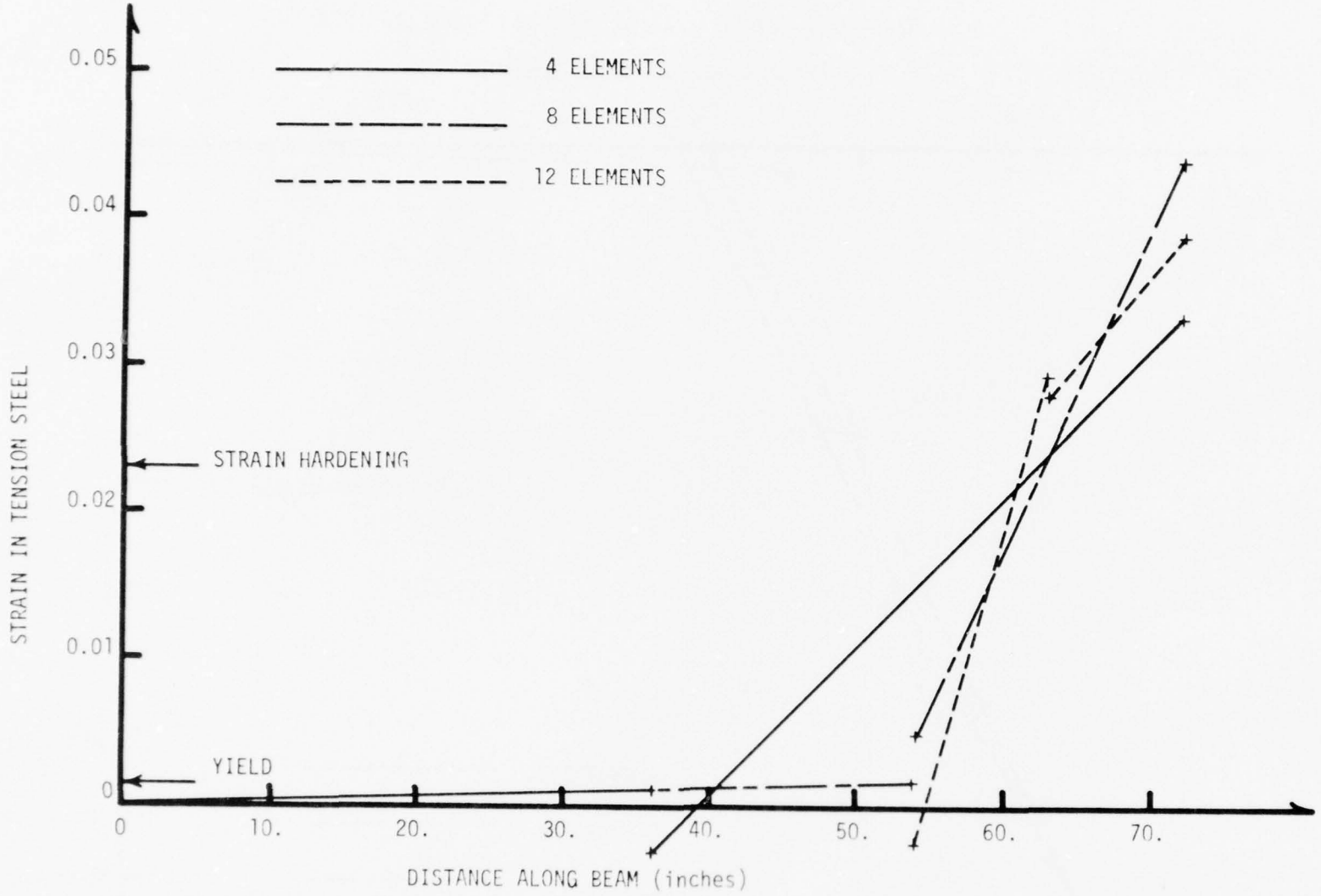

FIG. 23 STRAIN DISCONTINUITY - FIRST LOAD LEVEL

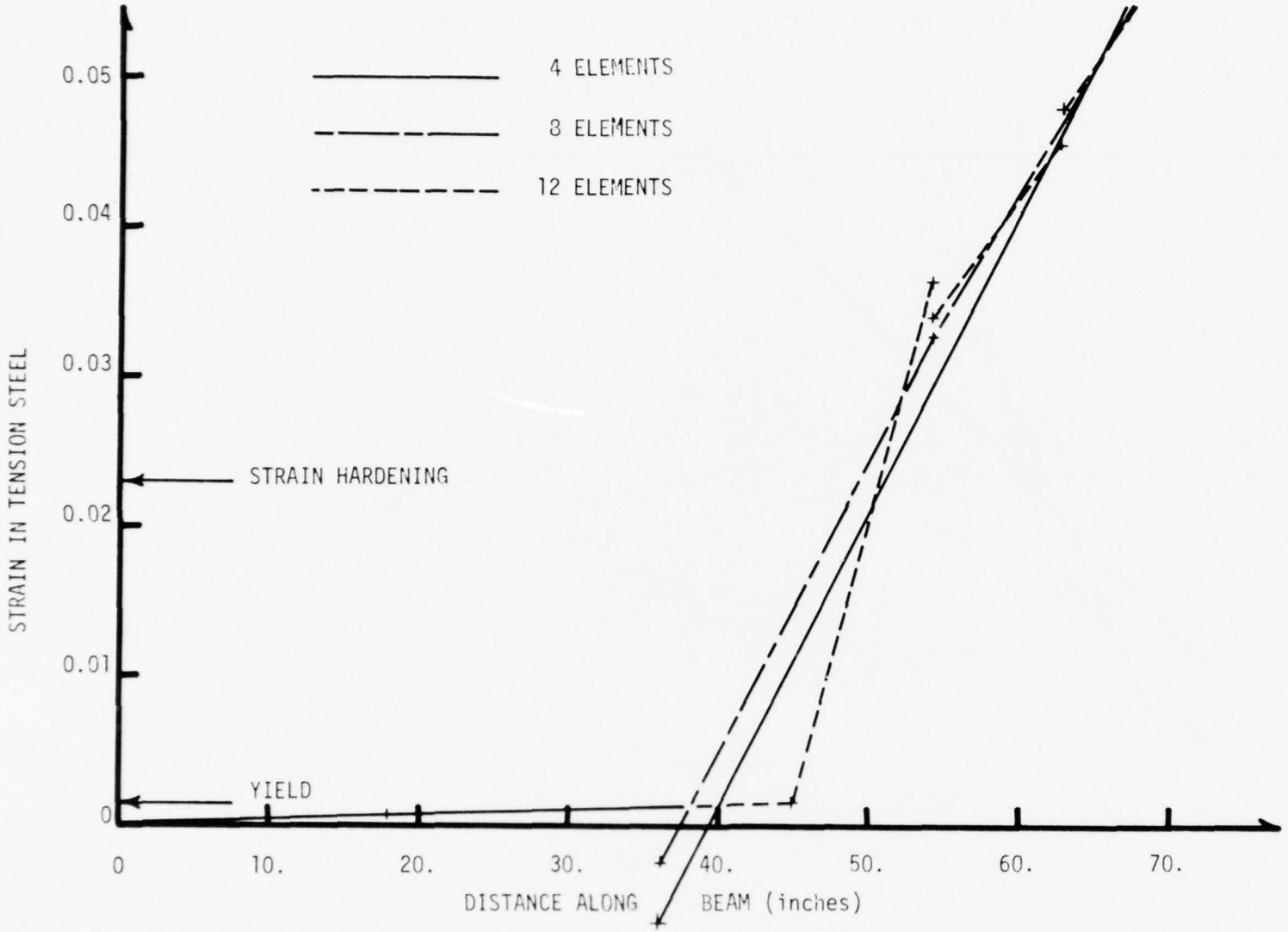

FIG. 24 STRAIN DISCONTINUITY - SECOND LOAD LEVEL

level, the strains change from yield to three times strain hardening within a distance of 1.35 times the depth of the beam. The average rate of change for both regions is essentially the same. The strains within the remaining portion of the beam are at or below yield strain.

These strain gradients must be modeled by the SINGER elements which are constrained to produce linear strain fields. It has been previously discussed (see section IV) that the continuum strain distribution in an element becomes complex and discretization errors grow when material properties are nonlinear and deformations are large. The lack of modeling capability which would provide for continuous strain distribution in the elements is reflected in the discontinuous characteristics that occur in these complex strain regions. The strain continuity can be maintained by elements if the continuum strain field can be closely approximated by a linear distribution. This is demonstrated in the less severely strained regions of the beam represented in figures 23 and 24 .

The computational reason for the possibility of the discontinuity in strains at adjacent sections is that the minimization process does not include any direct control on strain values. The generalized coordinate values corresponding to an equilibrium configuration are determined by the minimization of the total system energy. The total energy is composed of the summation of the individual element energies and the contribution from the applied forces and the inertia forces. The convergence of the minimization process is controlled by a measure of the largest stepsize used in the search at a point in the configuration space. The error associated with a converged state is determined by a

dimensionless measure of the largest value of the residual forces at the joints. Both of these process measurements are macro quantities. There is no direct measurement of strain used to control the process or to measure errors. Its effect enters only indirectly through the element energy computations. Hence, strain continuity between elements is possible, but certainly not guaranteed by the process itself.

SHEAR EFFECTS IN REINFORCED CONCRETE

The complete planar response of a beam-column member includes axial, flexural and shear deformation components, with the flexural and shear deformation comprising the transverse displacement. For most commonly used dimensions, the flexural contribution dominates the tranverse displacement. However, it is commonly known from the analysis of two dimensional stress fields that members with relatively large depth - length ratios (deep beams) may have a significant part of the transverse displacement contributed by the shear deformation component of the response. In addition, the total shear deformation in reinforced concrete deep beam members loaded to failure may be affected by internal concrete destruction and slippage associated with the growth of inclined cracks, since the failure state may be significantly larger than the initial cracking load [27].

The element model in SINGER includes axial and flexural deformation components, but it does not include shear deformation. Consequently, the response of any member is predicted according to the deformation coordinates $\bar{u}_1$, $\bar{u}_2$, $\bar{u}_3$, and $\bar{u}_4$ (see figure 7). For the line element used in SINGER,

shear deformation could be included by an indirect procedure; i.e., the shear deformation could be approximated from an average shear strain distribution at a section corresponding to a shear force which is required for equilibrium of the forces acting on the element. This approximation could also be incorporated in the transverse deformation function. However, the resulting expression is based on the linear material range. The extension into the inelastic material response plus the absence of test data for this effect in reinforced concrete create sufficient uncertainties so that the resulting shear deformation prediction was judged to be unreliable compared to the other deformation components in the element.

The effect of shear on the failure of an element is included in the failure criteria by an indirect procedure [1]. The purpose is to determine the force conditions which most probably cause a diagonal cracking failure state within an element. It is an indirect procedure based on experimental data, since there is no way to relate the shear force at a section with the corresponding strain state of the element. These criteria also include the effect of web reinforcement.

To demonstrate that the SINGER element model is not capable of accurately predicting the response of members which have a significant shear deformation, four deep beam test problems were studied. The comparison basis for the predicted response was obtained from experimental test results published by dePaiva and Siess [27]. The four problems correspond to their beam identifications noted G33S-11, G33S-12, G33S-31, and G33S-32. The beams G33S-11, 12 are referred to as beam (a.), and G33S-31, 32 are referred to as beam (b.). The physical details are summarized in figure

25; the response comparisons are plotted in figures 26, 27 and 28. The functional comparison relates the total applied load to the central transverse deflection for each beam to failure, shown in figures 26 and 27. Figure 28 shows a comparison of the strain at the center of the tensile reinforcing steel. In all cases it is clear that the SINGER element is much stiffer (less deformation at the same load level). Since the SINGER element includes only the flexural transverse deflection, a significant shear deformation is indicated in the test results (more than 50 percent of the total transverse deflection for all four cases). The central strain values of figure 28 support these observations, but the difference between the predicted and experimental values are relatively smaller, indicating closer agreement.

The implementation of the SINGER failure criteria for these problems produced predictions of the shear effects on element failure. These results were compared with the experimental inclined cracking load, shown below.

Beam	Load at Inclined Cracking (Kips)			
	With Web Reinf.		Without Web Reinf.	
	SINGER	Experimental	SINGER	Experimental
(a.)	20.0	12.90	2.0	13.32
(b.)	13.0	16.96	1.0	16.96

In SINGER, the initial detection of an inclined crack in a element without web reinforcement is indicated as a shear failure. For an element with web reinforcement, the failure is indicated after the web reinforcement yields. The experimental values tabulated above do not indicate failure;

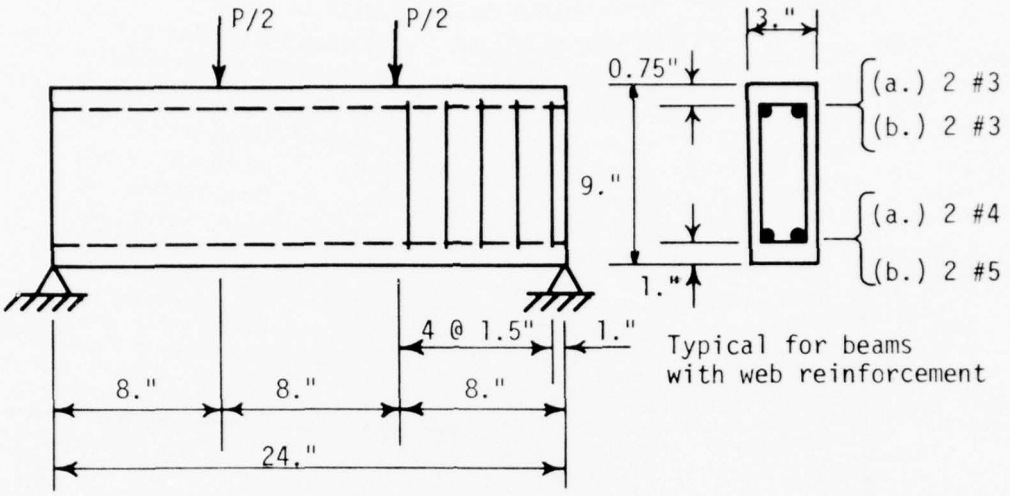

Material Properties:

Beam	Material Property	Stress Value (ksi)	
		With Web Reinf.	Without Web Reinf.
(a.)	f_c'	2.89	3.38
	f_y (tens.)	47.3	47.3
	f_y (compr.)	51.5	51.5
(b.)	f_c'	2.91	2.89
	f_y (tens.)	44.2	45.2
	f_y (compr.)	50.3	50.3

f_c' = concrete strength in compression

f_y (tens.) = yield stress of tension steel

f_y (compr.) = yield stress of compression steel

FIG. 25 SYSTEM AND MATERIAL PROPERTIES FOR SHEAR EFFECTS

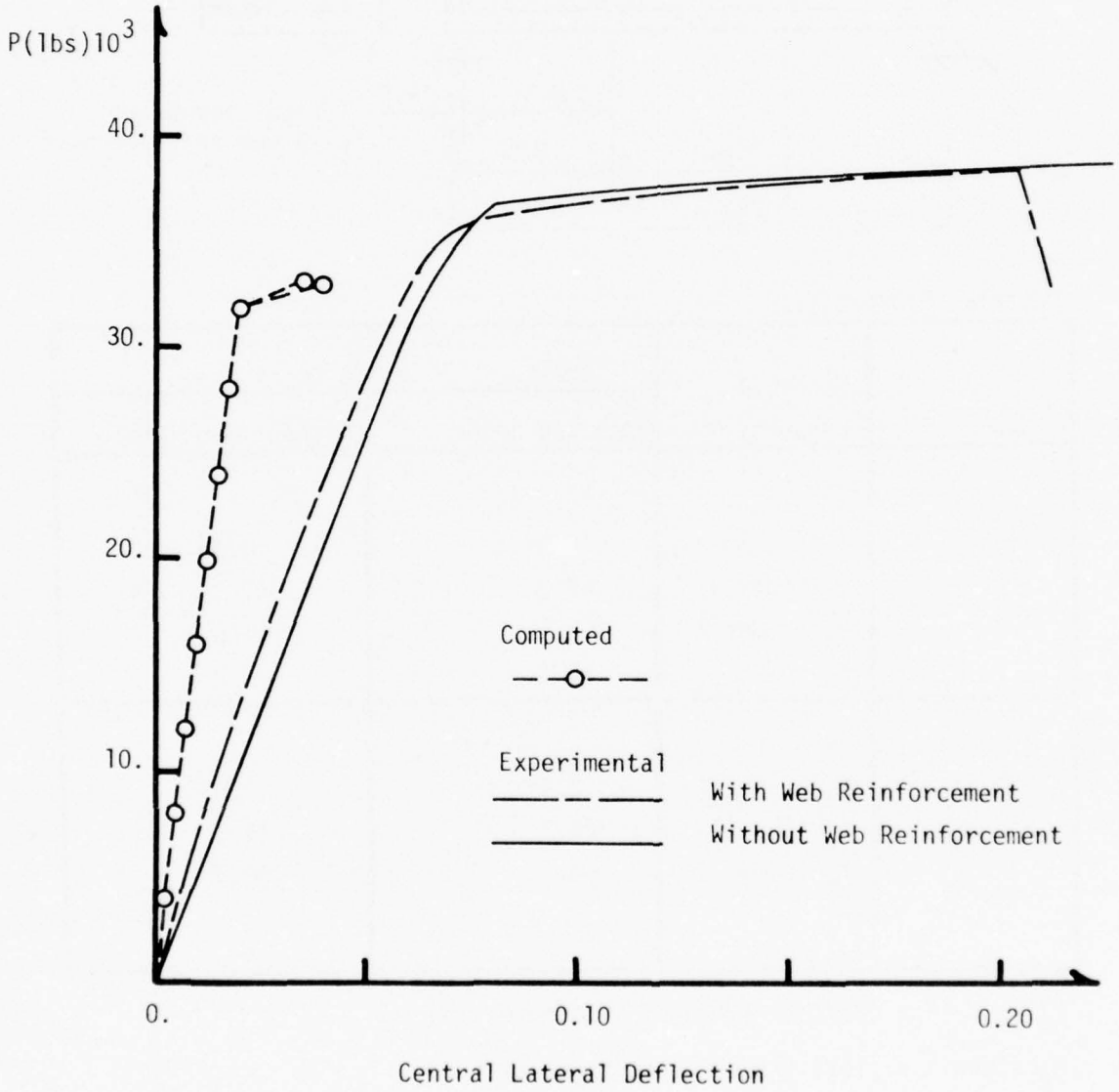

FIG. 26 RESPONSE COMPARISON FOR SHEAR EFFECTS - BEAM (a.)

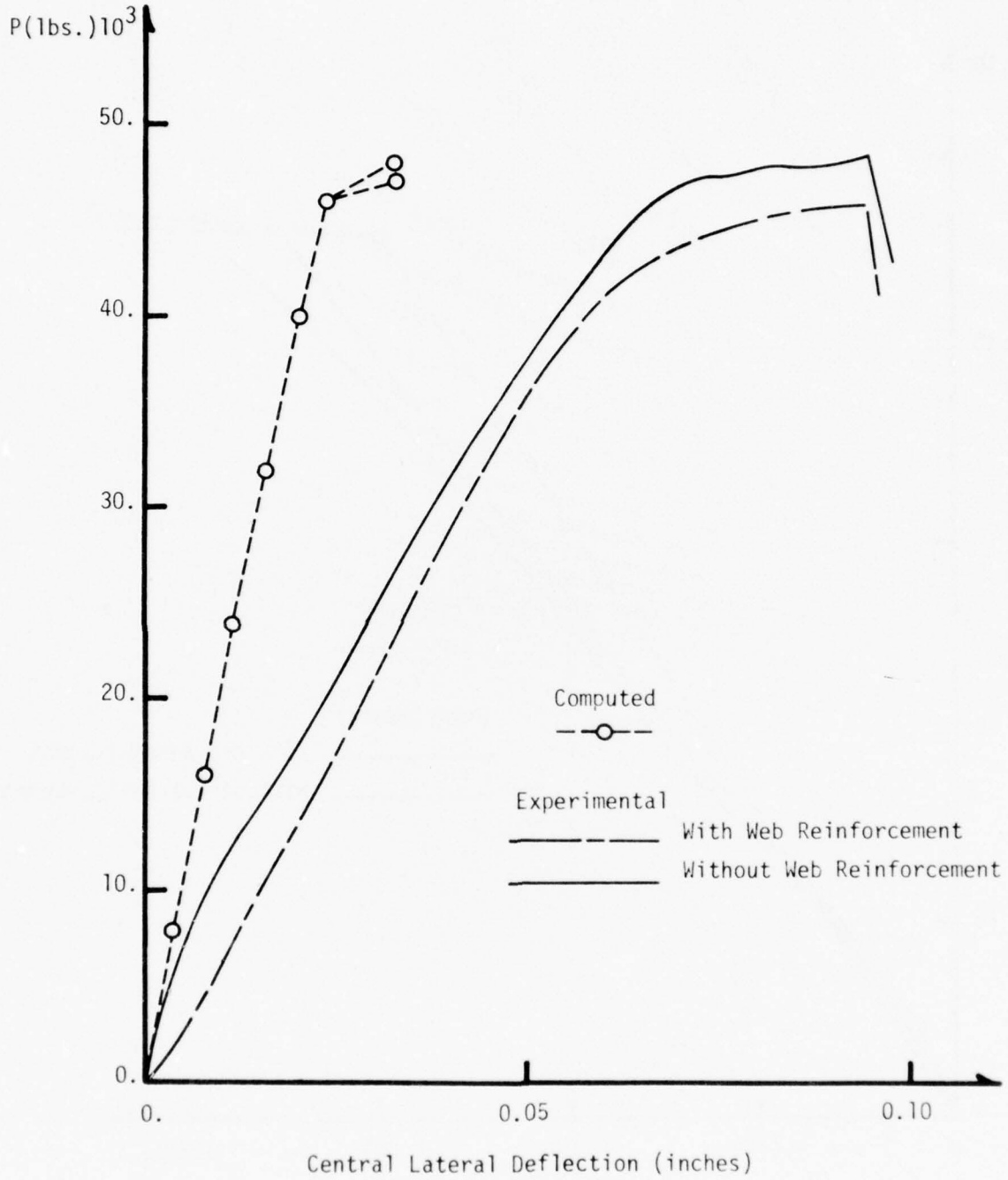

FIG. 27 RESPONSE COMPARISON FOR SHEAR EFFECTS - BEAM (b.)

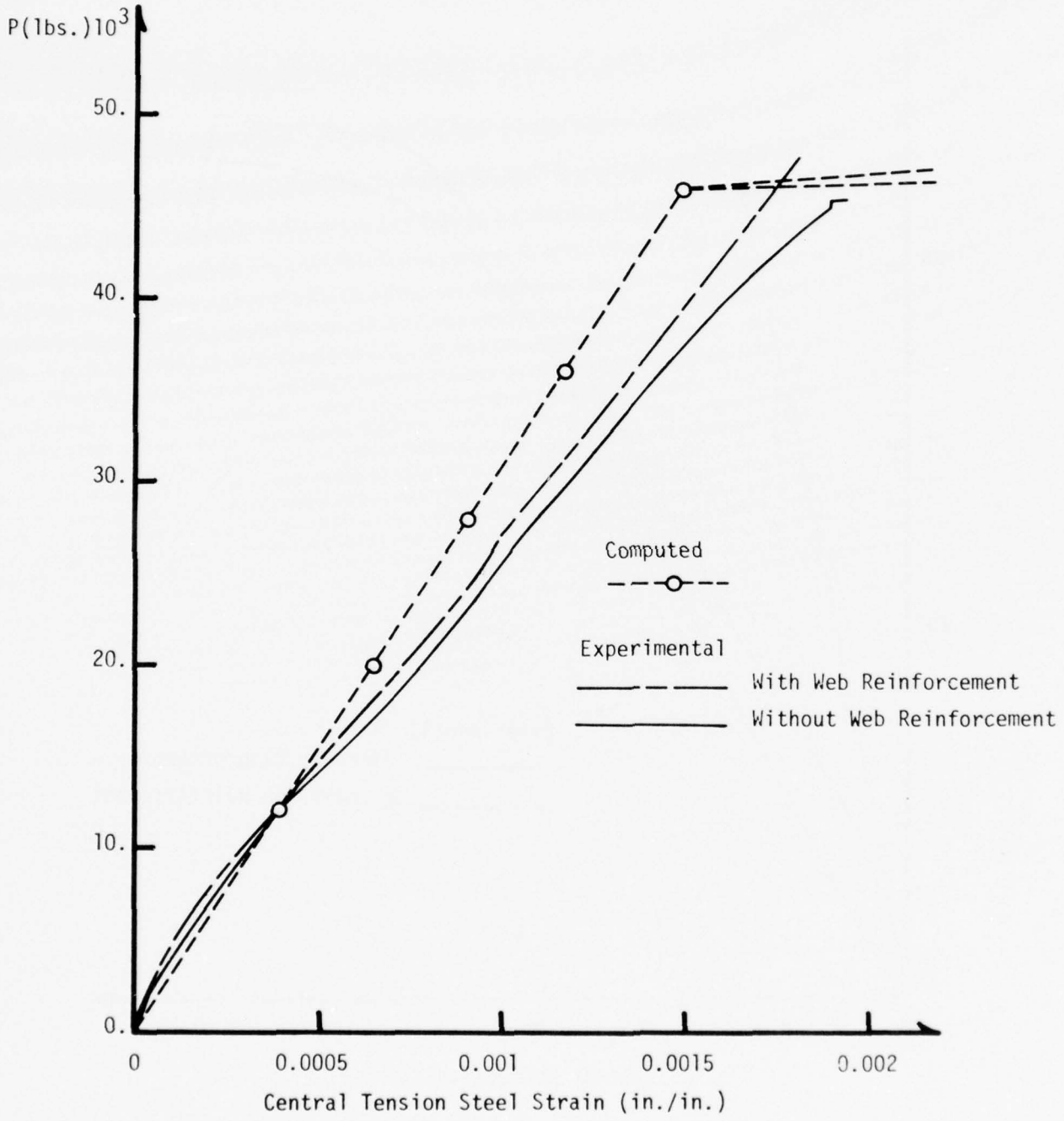

FIG. 28 TENSION STEEL STRAIN COMPARISON - BEAM (b.)

they do indicate the load at the detection of the first inclined crack. For the case of no web reinforcement, agreement is poor. The agreement for the case with web reinforcement is reasonable.

It should be noted that a thorough study of the failure criteria has not been attempted in this report. Such a study would be an extensive undertaking in itself, with a detailed knowledge of the capability and accuracy of the basic program serving as a mandatory prerequisite. The report has furnished the details of the refinement and demonstration of the current capability of SINGER.

SECTION VII

PROGRAM MODIFICATIONS AND SUGGESTED IMPROVEMENTS

The objective of this section is to document the significant modifications incorporated in the original version of the SINGER program [28] and to discuss improvements which should be made to provide more accurate and efficient response predictions.

PROGRAM MODIFICATIONS

The original version of the SINGER program was unable to solve a significant class of structural problems consistent with its potential capability, particularly those with reinforced concrete elements. This deficiency was due to several factors:

a. The scope of the program was extremely large, requiring many computational checks and much time to verify that all parts were working together correctly;

b. The time constraints left some of the subroutines virtually unchecked as computational units (primarily those involved with the internal energy computations for reinforced concrete elements);

c. A complex storage scheme of selected arrays, although efficient for computations, was difficult to implement and check;

d. Many people with varying programming experience contributed to the original program, creating a source of coding errors and inefficiency.

A considerable effort was required to expand the usable capacity of this program. The development of this task was influenced by the evolutionary growth of experience with the code. The first task involved removing coding errors and undefined variables so that the program would execute a set of input data. Once this was achieved, some modifications could be made to improve its efficiency and accuracy. There was no clear demarcation between these tasks, and an interaction was unavoidable.

The modifications made to the program cover a broad scope. The most significant contributions are listed in three categories: (1) correction of coding errors and computational errors;(2) improvements in computational efficiency; and(3) improvements in solution accuracy. The name in parentheses refers to the corresponding subroutine where the modification was made.

1. Correction of coding errors and computational errors:
    a. At least one undefined variable was detected in each of 10 subroutines. In many cases these were corrected by adding COMMON statements. (ADYN, BEAM, BOND, FAIL, FORK, GIDE, LEAF, OUTS, SECT, STEN).
    b. The subtraction of steel reinforcing bar area from concrete area was done incorrectly (COEN).
    c. The accumulation of the energy contribution from the reinforcing bars was done incorrectly (STEN).
    d. The default functions defining the stress-strain properties for both confined and unconfined concrete had some of the constant values incorrectly defined,

or they were inconsistent with the User's Guide (MATP).

e. A subscript computation for reference to a value stored in DATA was computed incorrectly. This particular error caused serious computational problems (COEN).

f. The computation for the energy associated with the steel reinforcing bars was incorrectly done due to an error in the Gaussian quadrature equations (STEN).

g. A subscript for the DATA array was incorrectly computed for use in generating forcing function values. An error in the forcing function value was caused for a forcing function defined by only two points (TABL).

h. An error occurred in the energy density computation for concrete for the special case when the previous and current strain values were identical. This error was also of a serious nature preventing correct convergence in the minimization process (CRET).

2. Improvements in computational efficiency:

a. Several logical IF decisions were rewritten to avoid awkward GO TO transfers.

b. Material data computations were removed from a subroutine within the solution process to avoid unnecessary repetition in the computations which were actually required to be done only once at the time of data input (COEN).

c. Many of the subroutines contained unreferenced statement numbers and redundant or duplicate statements, which were corrected.

d. Some segments were rewritten to use fewer statements to accomplish the same objective, particularly those using logical IF statements in a decision sequence.

e. At least one major subroutine was rewritten to avoid unnecessarily complicated organization, which was difficult to follow (ASAN).

f. Revisions were made in a few cases so that subroutines were called only when necessary for the given conditions rather than having the subroutine make the decision after being called.

3. Improvements in solution accuracy:

Two major revisions were implemented with the objective to remove or reduce the directional properties of the original element model.

a. The first revision reduced the axial strain contribution of the coupling term in the strain-displacement relation from a fourth order function in the x coordinate to a linear form to be consistent with the linear flexural strain contribution.

b. The second revision (documented in section V) completely redefined the basis for the element reference coordinate system. The deformation coordinates were redefined and the axial component of strain was again linearized with respect to the x coordinate.

Although both modifications were useful in improving the performance of the element within the system, the latter became a permanent

contribution to the program. The improvement in the element behavior was measured by observing the symmetry of element deformation and strains for a problem whose exact response had symmetric properties.

SUGGESTED IMPROVEMENTS

The current version of the SINGER code, although not yet completely operational, is capable of solving a broader class of problems than the original version, including reinforced concrete systems. The progress made in understanding and improving the program has also generated many ideas for further improvement. While some of these improvements are simply revisions to the form of output for a problem, others involve profound changes which would require extensive study before implementation. The ideas considered to be the most important are discussed below under four headings: (1) detection of errors and computational difficulties;(2) improvements in the form of input and output;(3) improvements in computational efficiency; and(4) improvements in solution accuracy.

1. Detection of errors and computational difficulties:
    a. The program should be capable of computing and displaying the components of the element and system energy quantities corresponding to a prescribed displacement configuration without including the minimization process for equilibrium. This would be useful for making checks on the internal energy computations.
    b. The default unconfined concrete material function should be revised to include a large strain value

corresponding to a small stress value at material point 7, similar to the form used for confined concrete. The area under the function between points 6 and 7 could be made sufficiently small to eliminate a significant energy contribution. The purpose would be to avoid the possibility of strain values exceeding the final material point during the solution process.

c. There should also be a check on user input material functions to prevent strains from exceeding the maximum strain point during a problem solution.

d. It may be useful to provide an option for implementing the failure criteria for a specific problem. Some forms of behavior may be more effectively studied by tracing the system response without incorporating local failure termination, and it may be helpful for checking the details of the failure criteria. Other nonrelated but essential computations performed in the subroutine (FAIL), such as stress resultant computations, should remain operational.

e. The subroutine which computes the internal energy in leaf spring elements (LEAF) is not consistent with the latest element model because the element deformation components have been redefined. This subroutine, if it is to be used, should be rewritten.

f. It may be important to have a provision to dump selected regions of the DATA and KDATA arrays to be able to study

their contents in conjunction with certain computational errors detected. This storage scheme has been the source of past errors and it is difficult to monitor.

2. Improvements in the form of input and output:

   a. The default confined concrete stress-strain values which are affected by the confinement factor ($\varepsilon_c(5)$, $f_c(5)$ and $\varepsilon_c(6)$) are never printed as a part of the output record. Their values are not known at the time of the function generation since the confinement factor depends on stirrup spacing, which is input after the material properties. Some provision should be made to print the complete function.

   b. Related to a. above, the user input function for confined concrete should be printed out in its entirety since it is not affected by the confinement property. Presently, the same three values are masked in the output as it is done for the default function since both functions are printed by the same statement.

   c. The complete applied force vector should be a part of the output record for each load increment regardless of the print level desired. In the present form, these forces are not printed for certain print level options.

   d. It would be desirable to include the option to print out results in a dynamic analysis only at specified time points to avoid extremely large volumes of output. Short messages could be printed between major output points to monitor the significant features of behavior.

3. Improvements in computational efficiency:

   a. The confinement factor is computed for every case which includes lateral reinforcement. However, it is used only for the default confined concrete function. It does not need to be computed for user input functions because their values are not affected by this factor.

   b. It could be helpful to develop a way to monitor the system response to provide information related to how close the system is to the conditions of the limit point.

4. Improvements in solution accuracy:

   a. A variable Gauss point mesh in an element would be an important feature to control the accuracy in the element energy computations (see section IV).

   b. It is necessary to study the behavior of higher order elements to be able to decide on the most efficient model for computing the system energy in the range of complex behavior, with particular emphasis on improving the interelement strain discontinuity problem (see section VI).

   c. It would be desirable to provide a way to monitor the change in slope for the individual elements and perhaps impose a slope change limitation based on the accuracy of element strain computations. It would provide the user with a warning when individual elements were excessively deformed. This monitor could also include

a check on the element strain gradients, and ultimately it could be related to a warning of possible strain discontinuities.

The experience gained by working with the SINGER program has established a firm confidence in its ability to solve problems within its intended capability. Although this potential has not been fully realized to date, it can ultimately be developed.

REFERENCES

1. Holzer, S. M., et al., SINGER: A Computer Code for General Analysis of Two-Dimensional Concrete Structures, AFWL-TR-74-228, Vol. I, Air Force Weapons Laboratory, Kirtland Air Force Base, NM, May 1975.

2. Bleich, F., Buckling Strength of Metal Structures, McGraw-Hill, 1952.

3. Karman, T. V., Collected Works of Theodore Von Karman, Vol. I, Butterworths Scientific Publications, London, 1956.

4. Broms, B., and Vient, I.M., "Ultimate Strength of Long Hinged Reinforced Concrete Columns," Journal of the Structural Division, ASCE, Vol. 84, ST 1, January 1958, p. 1510.

5. Chwalla, E., "Über die experimentelle Untersuchung des Tragverhaltens gedruckter Stabe aus Baustahl," Der Stahlbau, Vol. 7, 1934, p. 17.

6. Oliveira, E. R. A., "Theoretical Foundations of the Finite Element Method," International Journal of Solids and Structures, Vol. 4, 1968, p. 929.

7. Langhaar, H. L., Energy Methods in Applied Mechanics, John Wiley, 1962.

8. Timoshenko, S. P., and Gere, J. M., Theory of Elastic Stability, McGraw-Hill, 1961.

9. Jezek, K., "Die Tragfahigkeit des exzentrisch beanspruchten und des querbelasteten Druckstabes aus einem ideal plastischen Stahl," Sitzungsberichte der Akademie der Wissenschaften in Wien, Abt. II a, Vol. 143, 1934.

10. Timoshenko, S. P., History of Strength of Materials, McGraw-Hill, 1953.

11. Chwalla, E., "Die Stabilitat zentrisch und exzentrisch gedruckter Stabe aus Baustahl," Sitzungsberichte der Akademie der Wissenschaften in Wien, Abt. II a, 1928.

12. Chen, W. F., "General Solution of Inelastic Beam-Column Problem," Journal of the Engineering Mechanics Division, ASCE, EM4, August 1970, p. 421.

13. Chen, W. F., and Santathadaporn, S., "Curvature and the Solution of Eccentrically Loaded Columns," Journal of the Engineering Mechanics Division, ASCE, EM1, February 1969, p. 21.

14. Iyengar, S., and Chen, W. F., Computer Program for an Inelastic Beam-Column Problem, Fritz Engineering Laboratory Report No. 331.7, Lehigh University, Pa., 1970.

15. Bradshaw, J. C., Nonlinear Analysis of Plane Frames, Master Thesis, Virginia Polytechnic Institute and State University, May 1975.

16. Kopal, Z., Numerical Analysis, 2nd ed., Cahpman & Hall, 1961.

17. Shield, F., Numerical Analysis, Schaum Series, McGraw-Hill, 1968.

18. Lanczos, C., Applied Analysis, Prentice Hall, 1956.

19. Stroud, A. H., Secrest, D., Gaussian Quadrature Formulas, Prentice Hall Inc., Englewood Cliffs, N. J., 1966.

20. Krylov, V. I., Approximate Methods of Higher Analysis, Macmillan, New York, 1962 (Translated from Russian by A. H. Stroud).

21. Zienkiewicz, O. Z., The Finite Element Method in Engineering Science, McGraw-Hill, 1971.

22. Ivanova, A. N., "On Convergence of Sequences of Quadrature Formulas of Guass Type on an Infinite Interval, " Dokl. Akad, Nauk SSSR, 104, 1955, 169-172 (Russian).

23. Szegö, G., "Orthogonal Polynomials," Am. Math. Soc. Colloqium Publ., 23, 1959.

24. Hildebrand, F. B., Introduction to Numerical Analysis, McGraw-Hill, 1975.

25. Burns, N. H., and Siess, C. P., "Plastic Hinging in Reinforced Concrete," Journal of the Structural Division, ASCE, Vol. 92, No. ST 5, October 1966, p. 45.

26. Lane, G. E., Behavior of Reinforced Concrete Beams under Combined Axial and Lateral Loading, AFWL-TR-76-130, Air Force Weapons Laboratory, Kirtland Air Force Base, NM, 1976.

27. de Paiva, H. A. R. and Siess, C. P., "Strength and Behavior of Deep Beams in Shear," Journal of the Structural Division, ASCE, Vol. 91, No. ST 5, October 1965, p. 19.

28. Barker, R. M., et al., SINGER: A Computer Code for General Analysis of Two-Dimensional Concrete Structures, AFWL-TR-74-228, Vol. II, Air Force Weapons Laboratory, Kirtland Air Force Base, NM, May 1975.

ERRATA TO ORIGINAL REPORT

The work function, W, defined by Eq. 3.14 in reference 1 should be replaced by the energy function, E, which is defined as

$$E = \sum_{i=1}^{n} \left[\frac{6m_i}{\Delta t^2} \left(\frac{x_{bi}^2}{2} - \alpha_i x_{bi} \right) - (f_{bi} + f_{bi}^e) x_{bi} \right] + U \tag{1}$$

where

$$\alpha_i = x_{ai} + \dot{x}_{ai} \Delta t + \ddot{x}_{ai} \frac{\Delta t^2}{3} \tag{2}$$

The energy function assumes a stationary value if

$$\frac{\partial E}{\partial x_{bi}} = 0, \quad i = 1,2,\ldots,n \tag{3}$$

Eqs. 3 yield n equations of equilibrium of the form

$$m_i \ddot{x}_{bi} + \frac{\partial U}{\partial x_{bi}} = f_{bi} + f^e{}_{bi}, \quad i = 1,2,\ldots,n \tag{4}$$

where

$$\ddot{x}_{bi} = \frac{6}{\Delta t^2} (x_{bi} - \alpha_i) \tag{5}$$

Eq. 5 follows from Eqs. 3.4 and 3.5 in reference 1 with $t = \Delta t$; i.e., $\ddot{x}_{bi} = \ddot{x}_i(\Delta t)$.

DISTRIBUTION LIST

Dir.
DNA
ATTN: STSI
2 cy ATTN: SPSS
3 cy ATTN: STTL

DDR&E
ATTN: Asst. Dir., Strat. Wpns.

Dir.
DIA
ATTN: DIR-4C

Dir.
OSD, ARPA
ATTN: NMR

Cdr.
FC DNA
ATTN: FCPR

Ch.
LVLO
ATTN: FCTCL

JSTPS
ATTN: JLTW

CO
USACDC

CO
BRL
ATTN: AMXBR-TB

Ch. of Eng.
ATTN: DAEN-RDM

Dir.
USA Eng., WWES
3 cy

Dir.
NRL
ATTN: 2027

Cdr.
NSWC
ATTN: 730

NCEL
3 cy

HQ USAF
AFTAC
ATTN: TAP

HQ USAF
ATTN: SA
ATTN: SAMI
ATTN: PREE
ATTN: PREPB
ATTN: RDPQ, 1C370
ATTN: RDQSM, 1D425
ATTN: RDQS

AFCEC
ATTN: PREC

Dir., Nuc. Surety
ATTN: SN

AFSC
ATTN: DOB

TAC
ATTN: DEE
ATTN: LGMD

CINCSAC
ATTN: DEE
ATTN: DOXS
ATTN: XPFC

AFLC
ATTN: Mr. Edward G. Fink
20 cy ATTN: DEMG

ADC
ATTN: XPQY

AU
ATTN: ED, Dir., Civ. Eng.

AFIT
ATTN: Tech. Lib., Bldg. 640, Area B
ATTN: CES

USAFA
ATTN: DFSLB
ATTN: FJSRL, CC

AFML
ATTN: Tech. Lib.

AFFDL
ATTN: DOO, Lib.

SAMSO
10 cy ATTN: DEE

DISTRIBUTION LIST (Continued).

RADC
ATTN: Doc. Lib.

AFWL
ATTN: DE
ATTN: DES, 1Lt J. C. Bradshaw, III
20 cy ATTN: DES

AFOSR

Sandia Lab.
ATTN: Org. 3141

Dir. Ofc., LLL
ATTN: Tech. Info. Dept.

LLL
ATTN: Lib.

Dir., LASL
ATTN: Rpt. Lib.

Engineering Library
Air Force Institute of Technology

Engineering Library
University of California at Berkeley

Engineering Library
University of California at Los Angeles

Engineering Library
Colorado State University

Engineering Library
University of Colorado

Engineering Library
University of Illinois

Engineering Library
Massachusetts Institute of Technology

Engineering Library
University of Michigan

Engineering Library
Ohio State University

Engineering Library
Oregon State University

Engineering Library
Princeton University

Engineering Library
Stanford University

Engineering Library
Utah State University

Engineering Library
University of Utah

Department of Civil Engineering
Virginia Polytechnic Institute & State University
ATTN: A. E. Somers
ATTN: R. G. Galloway
50 cy ATTN: S. M. Holzer

Official Record Copy/1Lt J. C. Bradshaw, III, AFWL/DES